
OPEL: Optimal Transport Guided Procedure Learning

Sayeed Shafayet Chowdhury, Soumyadeep Chandra, and Kaushik Roy

Elmore Family School of Electrical and Computer Engineering

Purdue University, West Lafayette, IN 47907, USA

{chowdh23, chand133, kaushik}@purdue.edu

Abstract

Procedure learning refers to the task of identifying the key-steps and determining their logical order, given several videos of the same task. For both third-person and first-person (egocentric) videos, state-of-the-art (SOTA) methods aim at finding correspondences across videos in time to accomplish procedure learning. However, to establish temporal relationships within the sequences, these methods often rely on frame-to-frame mapping, or assume monotonic alignment of video pairs, leading to sub-optimal results. To this end, we propose to treat the video frames as samples from an unknown distribution, enabling us to frame their distance calculation as an optimal transport (OT) problem. Notably, the OT-based formulation allows us to relax the previously mentioned assumptions. To further improve performance, we enhance the OT formulation by introducing two regularization terms. The first, inverse difference moment regularization, promotes transportation between instances that are homogeneous in the embedding space as well as being temporally closer. The second, regularization based on the KL-divergence with an exponentially decaying prior smooths the alignment while enforcing conformity to the optimality (alignment obtained from vanilla OT optimization) and temporal priors. The resultant optimal transport guided procedure learning framework ('OPEL') significantly outperforms the SOTA on benchmark datasets. Specifically, we achieve 22.4% (IoU) and 26.9% (F1) average improvement compared to the current SOTA on large scale egocentric benchmark, EgoProceL. Furthermore, for the third person benchmarks (ProCeL and CrossTask), the proposed approach obtains 46.2% (F1) average enhancement over SOTA.

1 Introduction

The development of autonomous agents capable of reliably replicating human actions to accomplish certain end goals presents significant challenges. Traditional approaches would necessitate hard-coding tedious explicit instructions for each sub-task of the process (thus difficult to scale and generalize). A more efficient solution would involve the agent learning directly from observing multiple demonstrations of the assembly, without the need of any label. This motivates us to explore unsupervised procedure learning from videos. In the context of this work, procedure learning (PL) is conceptualized as the process of determining the key-steps and their correct sequential order to accomplish an overall task, as demonstrated across multiple video demonstrations [1, 2, 3].

PL analyzes multiple videos of a task as illustrated in Figure 1, in contrast to action-based tasks [4], which focus on a single video. The single-video approach is inapplicable to the identification of repetitive key-steps across videos. Moreover, action-based tasks typically neglect the sequencing of events, crucial for discerning an overall expected procedure composed of the sub-tasks. For instance, they fail to capture variations in the sequence of key-steps between videos V1 and V2 (Fig. 1). Other research efforts in video understanding that employ instructional videos include procedure planning [5], verifying sequences of procedures [6], and summarizing instructional content [7]. Additionally, unlike video alignment tasks [8], PL specifically aims to localize these essential steps within videos.

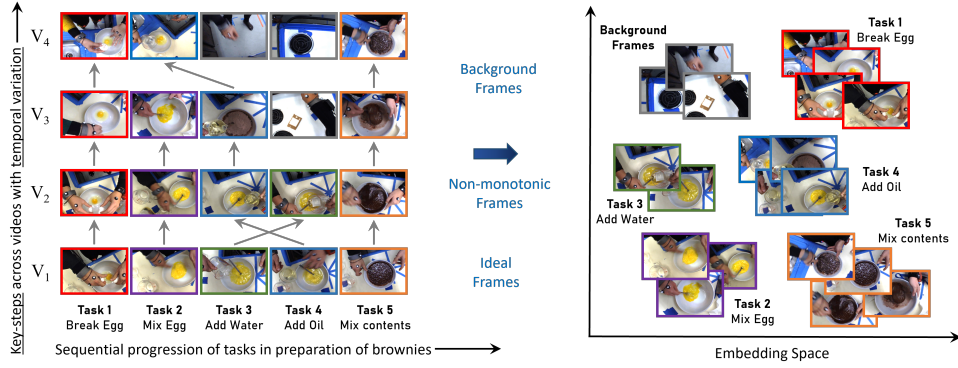


Figure 1: Key-steps required to prepare a brownie [17]. The sequences showcase temporal variations and corresponding key-step alignment challenges, namely (i) background frames (depicted as gray blocks), (ii) non-monotonic frames. OPEL aims to learn an embedding space where corresponding key-steps have similar embeddings while tackling the above challenges.

Much of the research on PL till now has been performed within the frameworks of supervised [9, 10, 11] and weakly supervised learning [12, 13, 14]. In a supervised setting, the reliance on per-frame annotations demands extensive manual labor. Conversely, weakly supervised methods involve using either ordered or unordered lists of key-steps. The generation of these lists requires either direct observation of the videos or specific heuristics, both of which pose significant scalability challenges [3]. Consequently, recent studies [1, 8] have shifted focus towards self-supervised learning, which do not require frame-wise labeling. Such a learning paradigm leverages the structured nature of accomplishing a complex task, which typically unfold in a predictable sequence of steps. For example, the act of preparing a "brownie" might involve breaking an egg, adding water, oil, mixing the contents, and then baking in the oven. The alignment of video frames is commonly performed in a monotonic manner [15], which presupposes a consistent order of actions across sequences. However, real-world sequences frequently deviate from this pattern, exhibiting temporal non-uniformities as depicted in Figure 1. These deviations can be categorized as follows: (i) background frames: frames irrelevant to the primary activity and should thus be excluded from alignment; (ii) redundant frames: these frames appear only in one sequence but not in others and do not contribute to the task; (iii) non-monotonic frames: these frames are characterized by a non-monotonic sequence of actions. Such frames challenge the assumption of monotonic progression and highlight the complexity of real-world activities. State-of-the-art (SOTA) methods adopt custom approaches to counter these irregularities such as removing background frames from processing [2], using extra information (e.g. gaze, depth) [16], or simply ignore them leading to suboptimal results [1].

To address the limitations of previous approaches, we relax the strict assumptions about the temporal sequence of actions and introduce a novel PL framework designed to learn temporal correspondences across videos. By treating instances of the sequences as samples from an unknown distribution, we formulate the task of computing the distance between them as an optimal transport (OT) [18] problem. The differentiable OT loss facilitates the alignment of non-monotonic sequences through frame-wise matching based on individual frame features. However, it typically overlooks the temporal smoothness and the inherent ordering relationships within the videos. To overcome this deficiency, we integrate two priors into the transportation matrix. First, the optimality prior favors the positions dictated by the OT, whereas the temporal prior discourages transport between temporally distant frames. Both these priors are modeled using a Laplace distribution with exponentially decaying probability from the corresponding centers. We introduce an additional virtual frame into the OT matrix to address background and redundant frames. Furthermore, to avoid the common issue of converging to trivial solutions in temporal video alignment [15], we employ a novel inter-video contrastive loss, which acts as a regularizer. Finally, the sub-tasks of each video are clustered in the embedding space using graphcut segmentation [19]. The overall framework, termed optimal transport guided procedure learning ('OPEL'), achieves SOTA results on both the ego and exocentric benchmarks. To summarize, our main contributions are-

- We propose a novel optimal transport based procedure learning framework that aligns frames with similar semantics together in an embedding space.

- To enhance the OT-based learning, we integrate optimality and temporal priors, both modeled using the Laplace distribution. These two priors also serve as regularizers. Furthermore, OPEL incorporates a novel inter-video contrastive loss for additional improvement.
- OPEL demonstrates substantial performance gains, achieving an average improvement of 22.4% in IoU and 26.9% in F1-score compared to the current SOTA on the EgoProeL benchmark.

2 Related Works

Representation Learning for Videos. Recent studies have explored various pretext tasks to facilitate representation learning through self-supervised or unsupervised approaches. Examples include temporal coherence and sequence ordering [20, 21, 22, 23, 24], predicting frames [25, 26, 27, 28, 29], and determining the directionality of time [30]. These methods typically derive signals from a constrained set of videos. In contrast, our objective is to discern and characterize key-steps of a certain task across multiple videos, expanding the scope and applicability of representation learning.

Self-Supervised Representations for Procedure Learning. Previous studies on PL have focused on developing methods for learning frame-level features [31, 3, 32, 33]. For instance, Kukleva et al. [32] enhance the representation space by utilizing relative timestamps of frames, while Vidal et al. [33] engage in predicting future frames along with their timestamps. Elhamifar et al. [3] apply attention mechanisms to individual frames to enhance feature learning. Similarly, Bansal et al. [1] leverage temporal correspondences across videos to generate signals and learn frame-level embeddings. The current SOTA model for egocentric PL [2] utilizes task-level graph representation to cluster semantically similar and temporally close frames. Despite these advancements, these methods often exhibit limitations in adequately modeling either temporal or spatial relationships within video sequences, especially in the presence of background and redundant frames. As a result, extra curated processing steps are required, resulting in additional layer of complexity and computation e.g. [2] depends on background frame removal to improve performance.

Multi-modal Procedure Learning. PL has also been used with multi-modal data such as (a) narrated text and videos [34, 35, 36, 37, 38, 39], (b) optical flow, depth and gaze information [16]. These studies typically rely on the assumption of a reliable alignment between video content and corresponding supporting modalities [34, 38, 39], an assumption that often proves inaccurate [31, 3] due to lack of synchrony among the modalities. Additionally, the dependence on imperfect Automatic Speech Recognition (ASR) systems necessitates subsequent manual corrections. Moreover, multiple modalities require additional memory and compute. In contrast, our framework exclusively leverages visual data, thereby circumventing the inaccuracies associated with multimodal alignment and enhancing scalability by eliminating the need for extra data modalities.

Video Alignment. can be efficiently addressed in synchronized settings using established methods like Canonical Correlation Analysis (CCA) [40] and soft-Dynamic Time Warping (DTW) [41]. A recent work [42] aligns videos by learning self-supervised representations from multiple viewpoints. However, the requirement for synchronized multi-view recordings limits its applicability. To tackle this challenge, [8] proposes a cycle consistency loss to establish frame correspondences, focusing primarily on local matches and not on the global temporal structure of the videos. Perhaps, works leveraging OT for visual analysis [43, 44, 45] are most related to our approach. But, such approaches do not address sequence alignment as we do. An exception is [46], which employs OT for videos, however their setup for evaluation is supervised fine-tuning for action segmentation, a fundamentally different task than unsupervised PL. As a result, [46] does not deal with temporal localization of the key-steps of a task nor their ordering, unlike us. Moreover, our modeling of priors using Laplace distribution and inter-video contrastive loss formulation are different from [46].

Learning Key-step Ordering. Most existing studies fail to account for variations in the ordering of key-steps required to complete a task, often assuming either a strict sequential order [31, 32, 33] or neglecting to model the sequence altogether [3, 47]. However, as illustrated in Figure 1, individuals frequently execute the same task in diverse manners, underscoring the need for a more flexible approach. To that end, OPEL is designed to identify and construct a unique key-step sequence for each video, thereby adapting to and inferring the specific ordering of the task.

3 OPEL Framework

Optimal Transport Formulation. OT provides a metric for assessing the dissimilarity between two probability distributions within a metric space [18]. By using the feature vectors from each entity and a distance matrix between them, it establishes correspondences that minimize total distance, also

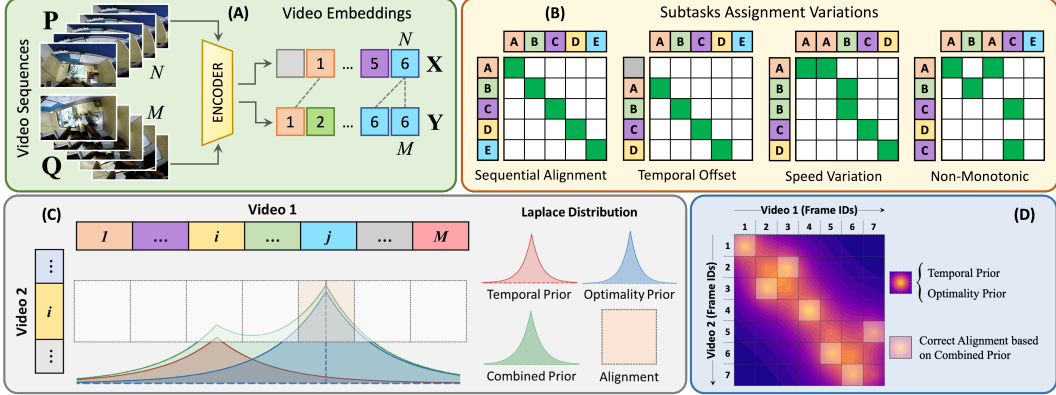


Figure 2: (A) The encoder generates frame-wise embeddings from videos, facilitating subsequent OT calculations. (B) Pair-wise scenarios captured through the assignment matrix- from strictly synchronized actions to temporal shifts and differing action speeds, to non-monotonicity. (C) 1-D depiction of alignment of a single frame (i -th) of Video 2 with its best match frame (j -th) of Video 1, based on the proposed priors. (D) 2-D representation of the optimal alignment of frame sequences.

ensuring optimality, separability, and completeness. Assume, the inputs are two sequences of video frames, $\mathbf{P} = [p_1, p_2, \dots, p_N]$ and $\mathbf{Q} = [q_1, q_2, \dots, q_M]$. We pass these through a deep encoder network (as illustrated in Fig. 2(A)) to obtain their respective embeddings, $\mathbf{X} = [x_1, x_2, \dots, x_N]$ and $\mathbf{Y} = [y_1, y_2, \dots, y_M]$. Let, (Ω, l) is a metric space, where $l : \Omega \times \Omega \rightarrow \mathbb{R}$ denotes the distance in Ω , and $P(\Omega)$ represents all Borel probability measures on Ω . Considering the elements of \mathbf{X} and \mathbf{Y} as independent samples, their probability measures can be written as, $f = \sum_{i=1}^N \alpha_i \delta_{x_i}$ and $g = \sum_{j=1}^M \beta_j \delta_{y_j}$, where δ_x denotes the Dirac mass at x , and α and β are the weights for the distributions f and g , respectively. Since there is no justification for assigning greater importance to one frame over another, initially we set $\alpha_i = \frac{1}{N}$ and $\beta_j = \frac{1}{M}$ for all i, j , leading to a feasible set of weight matrices defined as the transportation polytope [48], $U(\alpha, \beta) := \{\mathbf{T} \in \mathbb{R}_+^{N \times M} : \mathbf{T}\mathbf{1}_M = \alpha, \mathbf{T}^\top \mathbf{1}_N = \beta\}$. Here, t_{ij} can be interpreted to be proportional to the probability that x_i will be aligned to y_j . We start by computing the pairwise Euclidean distances between embedding vectors, $d(x_i, y_j) = \|x_i - y_j\|$ to form the $N \times M$ distance matrix, \mathbf{D} . The cost of transporting mass from f to g with a transport plan \mathbf{T} is quantified by the Frobenius inner product $\langle \mathbf{T}, \mathbf{D} \rangle$. Thus, the Wasserstein distance raised to the power p is: $W_p^p(f, g) = l_W(\alpha, \beta, \mathbf{D}) = \min_{\mathbf{T} \in U(\alpha, \beta)} \langle \mathbf{T}, \mathbf{D} \rangle$. We only consider $p = 1$, and drop p henceforth. To simplify the above optimization and make training feasible, Cuturi [48] introduced an entropy regularization, leading to the Sinkhorn distance,

$$l_\lambda^S(\alpha, \beta, \mathbf{D}) = \langle \mathbf{T}_\lambda, \mathbf{D} \rangle \quad \text{s.t. } \mathbf{T}_\lambda = \arg \min_{\mathbf{T} \in U(\alpha, \beta)} \langle \mathbf{T}, \mathbf{D} \rangle - \frac{1}{\lambda} h(\mathbf{T}), \quad (1)$$

where $h(\mathbf{T}) = -\sum_{i=1}^N \sum_{j=1}^M t_{ij} \log t_{ij}$ denotes the entropy of \mathbf{T} , and λ is the regularization parameter. The optimal solution for Eqn. (1) has the form [48], $\mathbf{T}_\lambda = \text{diag}(\kappa_1) \exp(-\lambda \mathbf{D}) \text{diag}(\kappa_2)$, where $\exp(-\lambda \mathbf{D})$ is the element-wise exponential of the matrix $-\lambda \mathbf{D}$, and $\kappa_1 \in \mathbb{R}^N$ and $\kappa_2 \in \mathbb{R}^M$ are the non-negative left and right scaling vectors to be obtained by the Sinkhorn fixed point iterations.

Regularization with Priors. The above formulation minimizes the cost of aligning two sequences, however it totally neglects the temporal ordering relationships inherent in videos, failing to leverage the temporal consistency. Typically, the alignment of multiple videos depicting the same activity should constrain the temporal position of one sequence to correspond closely with adjacent temporal positions of another sequence. Perfect alignment would render the transport matrix \mathbf{T} diagonal, but this strict requirement is impractical for real-world applications. As illustrated in Fig. 2(B), variations such as earlier commencement of activities, differing action speeds, or non-monotonic sequences complicate alignment. To address these challenges and achieve optimal alignment while accounting for temporal variations, we introduce two priors into the OT framework. Essentially, there are 2 factors in play - (i) optimality which tries to find the best match between frames irrespective of their temporal distance (which may result in temporally incoherent alignment), and (ii) the temporal factor which promotes transport between nearby frames only without considering their feature matching. We hypothesize that the optimal solution requires striking a balance between both, and thus propose to enhance the OT formulation by incorporating two specific priors addressing the above factors [46].

The first prior, termed the ‘Optimality Prior’, is introduced to effectively manage non-monotonic sequences. This prior leverages the transport matrix \mathbf{T} as delineated in Eqn. (1), which provides a preliminary indication of alignment between two video sequences. This matrix adapts dynamically to reflect the temporal variations observed across the sequences. Our approach uses this dynamic behavior to establish the optimality prior. We want the point representing the most likely alignment according to \mathbf{T} to have the highest likelihood, while the assignment probability decays along any perpendicular direction from this center. Specifically, we model this as a Laplace distribution,

$$\mathbf{Q}_o(i, j) = \frac{1}{2b} e^{-\frac{|d_o(i, j)|}{b}}, \quad \text{where } d_o(i, j) = \frac{|i/N - i_o/N| + |j/M - j_o/M|}{2\sqrt{1/N^2 + 1/M^2}}, \quad (2)$$

represents the average distance from (i, j) to the frame locations (i, j_o) and (i_o, j) that correspond to the optimal alignment as indicated by the transport matrix, and b is a scale parameter. Motivated by [46], we incorporate a second prior, termed the ‘Temporal Prior’, which promotes alignment of one sequence with elements in proximal temporal positions of the other sequence, thereby preserving the overall temporal structure and maintaining consistency in action order. This prior results in an assignment matrix characterized by peak values along the diagonal, with values diminishing perpendicular to the diagonal. Again, this scenario is modeled using a two-dimensional Laplace distribution, where the distribution along any line perpendicular to the diagonal is exponentially decaying, centered along the diagonal itself:

$$\mathbf{Q}_t(i, j) = \frac{1}{2b} e^{-\frac{|d_t(i, j)|}{b}}, \quad \text{where } d_t(i, j) = \frac{|i/N - j/M|}{\sqrt{1/N^2 + 1/M^2}} \quad (3)$$

is the distance from (i, j) to the diagonal. Inspired by [46], we merge these priors as,

$$\mathbf{Q}(i, j) = \phi \mathbf{Q}_t(i, j) + (1 - \phi) \mathbf{Q}_o(i, j), \quad (4)$$

where, ϕ serves as a dynamic weight, initially set to 1.0, and progressively reduced to 0.5 during training. This gradual adjustment of ϕ allows the model to adaptively improve its alignment based on the increasing fidelity of the OT predictions. Optimal alignment based on these priors is pictorially depicted in Fig.2(C, D). Note, the 1-dimensional alignment in Fig.2(C) is for demonstration only, our actual implementation is based on 2-dimensional distributional priors as shown in Fig.2(D).

Background and Redundant Frames. To effectively manage background and redundant frames, we integrate an additional ‘virtual frame’ within the transport matrix, following [46]. This serves as a placeholder for aligning any frame that do not match with the primary sequence, and allows OPEL to explicitly assign these non-contributing frames to the virtual frame, as shown in Fig. 4(B). The augmented transport matrix, now denoted as $\hat{\mathbf{T}} \in \mathbb{R}^{(N+1) \times (M+1)}$, includes an extra row and column to accommodate the virtual frame. Note, if the likelihood of a frame aligning with any salient frame falls below a predefined threshold, ζ , we assign that frame to the virtual frame.

Training Methodology. While the above formulation sounds promising, devising a differentiable framework to leverage these during training is pivotal. To that effect, following [46], we define 2 terms to effectively regularize $\hat{\mathbf{T}}$. To capture the essence of \mathbf{Q}_o , $\hat{\mathbf{T}}$ needs to be structured to highlight prominent values at locations corresponding to the most probable alignments,

$$M_o(\hat{\mathbf{T}}) = \sum_{i=1}^{N+1} \sum_{j=1}^{M+1} \frac{t_{ij}}{\frac{1}{2} d_m + 1}, \quad \text{where } d_m = \left(\frac{i - i_o}{N+1} \right)^2 + \left(\frac{j - j_o}{M+1} \right)^2 \quad (5)$$

Similarly, to conform to \mathbf{Q}_t , $\hat{\mathbf{T}}$ is expected to exhibit prominent values along its diagonal, reflecting temporally closely aligned frames; while off-diagonal elements should ideally possess diminished magnitudes. This sort of structural arrangement can be quantitatively assessed using:

$$M_t(\hat{\mathbf{T}}) = \sum_{i=1}^{N+1} \sum_{j=1}^{M+1} \frac{t_{ij}}{\left(\frac{i}{N+1} - \frac{j}{M+1} \right)^2 + 1} \quad (6)$$

Similar to Eqn. (4), the above 2 equations are combined as a regularizer on the transport matrix, $M(\hat{\mathbf{T}}) = \phi M_t(\hat{\mathbf{T}}) + (1 - \phi) M_o(\hat{\mathbf{T}})$. Such a structure is known as the inverse difference moment (IDM) [49, 46]. To encourage optimal alignment, $M(\hat{\mathbf{T}})$ of the learned $\hat{\mathbf{T}}$ should be maximized. In order to facilitate this and to ensure the smooth assignment of such matches, we define a modified feasible set for $\hat{\mathbf{T}}$ by incorporating two additional constraints into the set $U(\alpha, \beta)$,

$$U_{\xi_1, \xi_2}(\alpha, \beta) = \left\{ \hat{\mathbf{T}} \in \mathbb{R}_+^{N+1 \times M+1} \mid \hat{\mathbf{T}} \mathbf{1}_{M+1} = \alpha, \hat{\mathbf{T}}^\top \mathbf{1}_{N+1} = \beta, M(\hat{\mathbf{T}}) \geq \xi_1, \text{KL}(\hat{\mathbf{T}} \parallel \hat{\mathbf{Q}}) \leq \xi_2 \right\} \quad (7)$$

where $\text{KL}(\hat{\mathbf{T}} \parallel \hat{\mathbf{Q}}) = \sum_{i=1}^{N+1} \sum_{j=1}^{M+1} t_{ij} \log \frac{t_{ij}}{q_{ij}}$ is the Kullback- Leibler (KL) divergence between $\hat{\mathbf{T}}$ and $\hat{\mathbf{Q}}$, and $\hat{\mathbf{Q}}$ is same as Eqn. (4) but augmented with the virtual frame. So, the regularized Wasserstein distance between \mathbf{X} and \mathbf{Y} now becomes -

$$l_{\xi_1, \xi_2}^R(\mathbf{X}, \mathbf{Y}) = \min_{\hat{\mathbf{T}} \in U_{\xi_1, \xi_2}(\boldsymbol{\alpha}, \boldsymbol{\beta})} \langle \hat{\mathbf{T}}, \mathbf{D} \rangle. \quad (8)$$

The above optimization can be efficiently solved by considering its dual. As such, we incorporate two Lagrange multipliers, $\lambda_1 > 0$ and $\lambda_2 > 0$, to obtain the dual of Eqn. (8) as-

$$l_{\lambda_1, \lambda_2}^R(\mathbf{X}, \mathbf{Y}) := \langle \hat{\mathbf{T}}_{\lambda_1, \lambda_2}, \mathbf{D} \rangle, \text{ s.t. } \hat{\mathbf{T}}_{\lambda_1, \lambda_2} = \arg \min_{\hat{\mathbf{T}} \in U(\boldsymbol{\alpha}, \boldsymbol{\beta})} \langle \hat{\mathbf{T}}_{\lambda_1, \lambda_2}, \mathbf{D} \rangle - \lambda_1 M(\hat{\mathbf{T}}) + \lambda_2 \text{KL}(\hat{\mathbf{T}} \parallel \hat{\mathbf{Q}}). \quad (9)$$

The optimal $\hat{\mathbf{T}}_{\lambda_1, \lambda_2}$ that optimizes Eqn. (9) is $e^{\text{diag}(-\frac{1}{2} - \frac{\mu}{\lambda_2})} \mathbf{K} e^{\text{diag}(-\frac{1}{2} - \frac{\nu}{\lambda_2})}$, where $\mathbf{K} = [q_{ij} e^{\frac{1}{\lambda_2} (s_{ij}^{\lambda_1} - d_{ij})}]_{ij}$, $s_{ij}^{\lambda_1} = \lambda_1 \left(\frac{1}{(\frac{i}{N+1} - \frac{j}{M+1})^2 + 1} + \frac{1}{\frac{1}{2} d_m + 1} \right)$, d_m given by Eqn.(5), and μ and ν are the dual variables for the two equality constraints $\hat{\mathbf{T}} \mathbf{1}_{M+1} = \boldsymbol{\alpha}$, and $\hat{\mathbf{T}}^T \mathbf{1}_{N+1} = \boldsymbol{\beta}$, respectively. The detailed derivation of this optimal $\hat{\mathbf{T}}_{\lambda_1, \lambda_2}$ is provided in appendix section A.1.

Contrastive Regularization. Incorporating temporal priors into the video alignment processes often leads to trivial solutions [41, 46]. So, following [41, 1], we utilize the Contrastive-Inverse Difference Moment (C-IDM) loss to further regularize the training. This loss is characterized by,

$$I(\mathbf{X}) = \sum_{i=1}^{N+1} \sum_{j=1}^{M+1} (1 - \mathcal{N}(i, j)) \gamma(i, j) \max(0, \lambda_3 - d(i, j)) + \mathcal{N}(i, j) \frac{d(i, j)}{\gamma(i, j)}, \quad (10)$$

where $\gamma(i, j) = (i - j)^2 + 1$, $d(i, j) = \|\mathbf{x}_i - \mathbf{x}_j\|$, $\mathcal{N}(i, j)$ is a neighborhood function defined as: $\mathcal{N}(i, j) = 1$, if $|i - j| \leq \delta$ and 0 otherwise, δ is a predefined window size, λ_3 is a margin parameter. The preceding C-IDM loss is an intra-video loss. Additionally, we incorporate an inter-video contrastive loss guided by OT to further regularize the training process. Specifically, this novel loss component contrasts pairs of videos based on their similarity as quantified by the OT matrix. We find, $x_{\text{best}}(i) = \arg \max_j \hat{\mathbf{T}}_{\lambda_1, \lambda_2}$ and $x_{\text{worst}}(i) = \arg \min_j \hat{\mathbf{T}}_{\lambda_1, \lambda_2}$. Likewise, $y_{\text{best}}(j) = \arg \max_i \hat{\mathbf{T}}_{\lambda_1, \lambda_2}$ and $y_{\text{worst}}(j) = \arg \min_i \hat{\mathbf{T}}_{\lambda_1, \lambda_2}$ are calculated. Then, the best distance is computed as the average of squared differences between matched pairs, scaled by a temperature factor: $\text{best_distance} = \frac{1}{\text{temperature}} \cdot \left(\frac{1}{N} \sum_{i=1}^N \|\mathbf{x}_i - \mathbf{y}_{x_{\text{best}}(i)}\|^2 + \frac{1}{M} \sum_{j=1}^M \|\mathbf{y}_j - \mathbf{x}_{y_{\text{best}}(j)}\|^2 \right)$. Similarly, the worst distance is: $\text{worst_distance} = \frac{1}{\text{temperature}} \cdot \left(\frac{1}{N} \sum_{i=1}^N \|\mathbf{x}_i - \mathbf{y}_{x_{\text{worst}}(i)}\|^2 + \frac{1}{M} \sum_{j=1}^M \|\mathbf{y}_j - \mathbf{x}_{y_{\text{worst}}(j)}\|^2 \right)$. Finally, the inter-sequence loss is computed using the cross-entropy over the best and worst distances:

$$\text{loss_inter} = F_{\text{cross_entropy}} \left(\begin{bmatrix} \text{best_distance} \\ \text{worst_distance} \end{bmatrix}, \begin{bmatrix} 0 \\ 1 \end{bmatrix} \right). \quad (11)$$

Ideally, we want each frame embedding \mathbf{x}_i , to align highly to its best match from \mathbf{Y} . So the best distance should be as close to 0 as possible, at the same time, we maximize its distance from the unmatched frame embeddings, and the same holds true for \mathbf{y}_j s. As a result, our proposed inter-video loss (Eqn. (11)) promotes learning disentangled representations. So, the overall loss for OPEL combines the regularized OT loss (Eqn. (9)) with the contrastive regularization terms,

$$L_{\text{OPEL}}(\mathbf{X}, \mathbf{Y}) = c_1 * l_{\lambda_1, \lambda_2}^R(\mathbf{X}, \mathbf{Y}) + c_2 * (I(\mathbf{X}) + I(\mathbf{Y})) + c_3 * \text{loss_inter}. \quad (12)$$

Clustering and Key-step Ordering. After learning the embeddings, our goal is to localize the key-steps required for PL. We frame this problem as multi-label graph-cut segmentation [50]. The node set V of the graph includes k terminal nodes representing the key-steps and non-terminal nodes corresponding to the number of frames, which are derived from the embeddings produced by the embedder network. Upon constructing the graph, we apply α -Expansion [19] to identify the minimum cost cut, utilizing the results to assign frames to k labels. To deduce the sequential order of key-steps, we first compute the normalized time for each frame in a video, following [1]. Subsequently, the temporal instant for each cluster is determined by calculating the average normalized time for frames allocated to that cluster. Clusters are then sequenced in ascending order of their average time, thus outlining the sequence of key-steps of a video. Upon establishing the key-step order for all videos associated with the same task, we generate a ranked list based on the frequency at which subjects adhere to a specific sequence. The most commonly observed order is placed at the top of this list. This methodological approach allows us to discern various sequential orders of key-steps of a task.

4 Experiments and Results

Datasets. In contrast to previous research that predominantly utilized either 1st person or 3rd person viewpoints for PL, we incorporate datasets from both perspectives. For 3rd person view, we utilize established benchmark datasets, namely CrossTask [11] and ProceL [3]. CrossTask features 213 hours of video footage spanning 18 primary tasks, totaling 2763 videos. ProceL includes 47.3 hours of video from 12 varied tasks, comprising 720 videos. To evaluate the effectiveness of our proposed OPEL framework, we apply it to the 1st-person EgoProceL benchmark [1], which contains 62 hours of egocentric video recordings from 130 subjects engaged in 16 tasks. Detailed information on individual datasets is provided in Table A2 of appendix.

Evaluation. Unless specified differently, we assess OPEL as per the current SOTA [1, 2]. We compute the framewise scores for each key-step separately and then take the mean of the scores over all the key-steps, reporting both the F1-score and the Intersection over Union (IoU). The F1-score is defined as the harmonic mean of precision and recall. Precision is calculated as the ratio of the number of frames correctly predicted as key-steps to the total number of frames labeled as key-steps. Recall is determined by the ratio of correctly predicted key-step frames to the total number of actual key-step frames. Following the methodology in [1, 2, 31, 3, 47], we employ the Hungarian algorithm [51] to derive a one-to-one mapping between the ground truth and the predictions.

Table 1: Results using EgoProceL [1] demonstrate the superior performance of OPEL. The results in bold and underline denote the highest and second-highest values in a column, respectively.

	EgoProceL											
	CMU-MMAC [17]		EGTEA-GAZE+[52]		MECCANO[53]		EPIC-Tents[54]		PC Assembly		PC Disassembly	
	F1	IoU	F1	IoU	F1	IoU	F1	IoU	F1	IoU	F1	IoU
Random	15.7	5.9	15.3	4.6	13.4	5.3	14.1	6.5	15.1	7.2	15.3	7.1
Uniform	18.4	6.1	20.1	6.6	16.2	6.7	16.2	7.9	17.4	8.9	18.1	9.1
CnC [1]	22.7	11.1	21.7	9.5	18.1	7.8	17.2	8.3	25.1	12.8	27.0	14.8
GPL-2D [2]	21.8	11.7	23.6	14.3	18.0	8.4	17.4	8.5	24.0	12.6	27.4	15.9
UG-I3D [2]	28.4	15.6	25.3	14.7	18.3	8.0	16.8	8.2	22.0	11.7	24.2	13.8
GPL-w BG [2]	30.2	16.7	23.6	14.9	20.6	9.8	18.3	8.5	27.6	14.4	26.9	15.0
GPL-w/o BG [2]	31.7	17.9	27.1	16.0	20.7	10.0	19.8	9.1	27.5	15.2	26.7	15.2
OPEL (<i>Ours</i>)	36.5	18.8	29.5	13.2	39.2	20.2	20.7	10.6	33.7	17.9	32.2	16.9

Experimental Setup. We employ ResNet-50 (pretrained on ImageNet) as the embedder network. Inspired by [1], we train the embedder using pairs of training videos. Within these videos, we randomly select frames and optimize the proposed L_{OPEL} until convergence. The feature extraction is conducted from the Conv4c layer, and we subsequently create a stack of 2 context frames along the temporal dimension. Our video frames are resized to 224×224. The aggregated features are processed through two 3D convolutional layers, followed by a 3D global max pooling layer, two fully-connected layers, and a linear projection layer that outputs embeddings of 128 dimensions. All hyper-parameters are listed in Table A1. Our code is provided as part of the supplementary material.

Results on Egocentric View. Table 1 presents a comparative analysis between the SOTA techniques and OPEL applied to the large scale egocentric benchmark, EgoProceL. Results from tasks within CMU-MMAC and EGTEA G. have been aggregated and presented (detailed task-wise results are given in Table A4). It is important to highlight that EgoProceL represents a contemporary dataset specifically designed for egocentric procedure learning, thereby limiting the number of applicable approaches for fair comparison. Notably, OPEL outperforms the SOTA across most tasks. This superiority underscores the efficacy of the video representation learning through OT. Specifically, we achieve 22.4% (IoU) and 26.9% (F1) average improvement compared to current SOTA.

Results on Third-person View. We provide comparison between SOTA and OPEL on two distinct third-person datasets [3, 11] in Table 2. To ensure consistency in evaluation, we follow the evaluation protocol outlined in the SOTA prior arts [1, 2]. Once again, we perform better in almost all cases, with

Table 2: PL results on third-person datasets [3, 11]. P, R, and F1 represent precision, recall, F1-score.

	ProceL [3]			CrossTask [11]		
	P	R	F1	P	R	F1
Uniform	12.4	9.4	10.3	8.7	9.8	9.0
Alayrc <i>et al.</i> [34]	12.3	3.7	5.5	6.8	3.4	4.5
Kukleva <i>et al.</i> [32]	11.7	30.2	16.4	9.8	<u>35.9</u>	15.3
Elhamifar <i>et al.</i> [3]	9.5	26.7	14.0	10.1	41.6	16.3
Fried <i>et al.</i> [37]	-	-	-	-	28.8	-
Shen <i>et al.</i> [47]	16.5	31.8	21.1	15.2	35.5	21.0
CnC [1]	20.7	22.6	21.6	22.8	22.5	22.6
GPL-2D [2]	21.7	23.8	22.7	24.1	23.6	23.8
UG-I3D [2]	21.3	23.0	22.1	23.4	23.0	23.2
GPL [2]	22.4	24.5	23.4	24.9	24.1	24.5
STEPS [16]	23.5	26.7	24.9	26.2	25.8	25.9
OPEL (<i>Ours</i>)	33.6	36.3	34.9	35.6	34.8	35.1

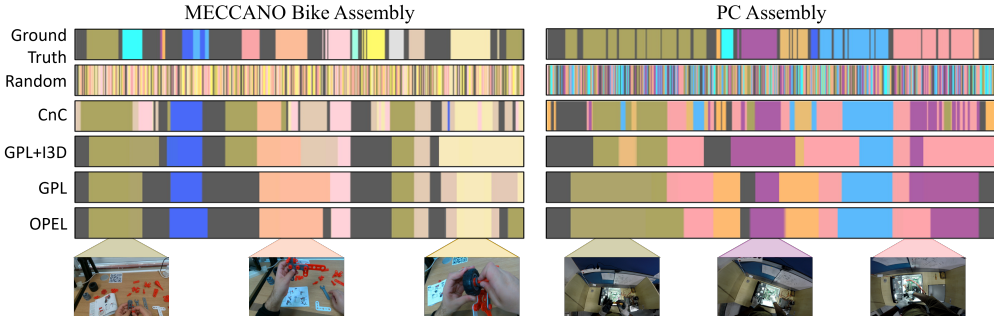


Figure 3: Qualitative results from MECCANO [53] and PC Assembly [1] tasks. Each sub-task is color-coded to represent different key-steps, while gray areas signify background elements. Notably, OPEL’s performance surpasses that of the SOTA networks, attributed to its ability to handle unmatched frames through the integration of a virtual frame, thus enhancing alignment accuracy.

46.2% (F1) average enhancement over SOTA. Note, [32, 3] predominantly allocate frames to a single key-step, resulting in elevated recall rates but concomitantly diminishing precision, consequently impacting the overall F-score. Additional detailed third-person results from CMU-MMAC [17], ProceL [3] and CrossTask [11] are given in Table A3 and Table A5, respectively.

Qualitative Results. Fig. 3 illustrates the qualitative PL outcomes of the baselines and OPEL. Higher match with the ground truth in our case (the bottom row) depicts the usefulness of OPEL. Additionally, we depict the alignment of two sequences in Fig. 4(B), showcasing accurate alignment despite temporal variations, with correct matches indicating consistent action frame alignment and redundancy handling, affirming the reliability of our model.

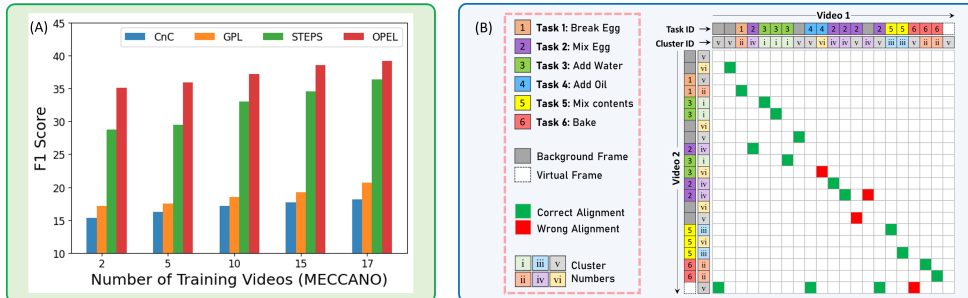


Figure 4: (A) Impact of training data quantity on encoder training. (B) Example alignment of two videos with corresponding key-step clusters from the Brownie task [17].

Comparison with Multimodal Models. While we only use videos for training, our results are competitive with models using multiple modalities. On the egocentric EgoProcel dataset, we perform comparably or even better (4 out of 6 datasets) compared to the multimodal SOTA model, STEPS [16], as shown in Table 3. Note, STEPS uses gaze and depth data during training, thus enhancing its results on EPIC-Tents. We also outperform [47, 34] (Table 2), which use narrations with video.

Table 3: Comparison with models with multimodal input. Note, STEPS [16] uses additional data (optical flow, gaze, depth) for training, while we use just the visual modality.

	CMU-MMAC		EGTEA-GAZE+		MECCANO		EPIC-Tents		ProceL		CrossTask	
	F1	IoU										
STEPS [16]	28.3	11.4	30.8	12.4	36.4	18.0	42.2	21.4	24.9	15.4	25.9	14.6
OPEL	36.5	18.8	29.5	13.2	39.2	20.2	20.7	10.6	34.9	21.3	35.1	21.5

5 Ablation Study

Effectiveness of L_{OPEL} . We analyze the effectiveness of the proposed loss by replacing or combining with other SOTA losses used for PL - TCC [8], LAV [41], and CnC [1]. Overall, the proposed L_{OPEL} outperforms previous approaches as shown in Table 4. This enhancement can be attributed to the flexibility in modeling sequences provided by OT. Furthermore, ablation results on all the loss components of L_{OPEL} are provided in Table 5, where we show the contribution of each factor individually to analyze their effect on the overall result. Comparing row 3 with row 9, we observe, the priors jointly play a critical role; as without them (row 3), the F1 and IoU scores drop by ~ 5 points.

Specifically, the optimality prior has a significant impact (~ 2 point), while the temporal prior affects the score by ~ 1 point. Similar to the combined priors, the intra and inter-video contrastive losses together (row 6 vs row 9) have a significant effect (~ 3.5 points) on the overall performance. The individual effect of virtual frame is negligible as it only plays a role in case of excessive background frames - a scenario that is not prevalent in most datasets. Furthermore, due to the IDM structure of $M(\hat{T})$, the \hat{T} and \hat{Q} are similar by formulation. This results in $KL(\hat{T} \parallel \hat{Q})$ to be already small. As a consequence, adding the KL divergence as a standalone loss component in the proposed pipeline has a minimal impact. Overall, while some loss components may have a smaller individual impact, they do contribute to performance improvements, even if incrementally. Therefore, our proposed approach incorporates all of them to achieve the best possible results.

Table 4: Comparison of effectiveness of L_{OPEL} with other losses.

	CMU-MMAC [17]			MECCANO [53]			EGTEA-GAZE+ [52]			PC Assembly [1]		
	P	F1	IoU	P	F1	IoU	P	F1	IoU	P	F1	IoU
TCC + PCM [8]	18.5	19.7	9.5	15.1	17.9	8.7	17.5	19.7	8.8	19.9	21.7	11.6
LAV + TCC + PCM [41]	18.8	19.7	9.0	13.4	15.6	7.3	16.4	18.6	7.5	21.6	21.1	10.8
LAV + PCM [41]	20.6	21.1	9.4	14.6	17.4	7.1	17.4	19.1	8.0	21.5	22.7	11.7
TC3I + PCM (CnC) [1]	21.6	22.7	11.1	15.5	18.1	7.8	19.6	21.7	9.5	25.0	25.1	12.8
OT + TCC	28.8	32.6	15.6	25.2	34.5	17.5	22.6	26.7	11.2	27.8	28.2	15.6
OT + LAV	30.2	34.7	16.8	26.7	36.2	18.8	23.1	27.8	12.4	30.2	30.9	16.8
OT + TCC + LAV	27.6	31.2	15.3	23.8	33.6	16.1	21.8	25.4	10.5	28.1	28.4	14.7
OPEL (<i>Ours</i>)	32.8	36.5	18.8	28.9	39.2	20.2	24.3	29.5	13.2	32.5	33.7	17.9

Table 5: Analysis of the impact of each term in L_{OPEL} on the overall performance.

Intra-Video	Inter-Video	KL Divergence	Temporal Prior	Optimality Prior	Virtual Frame	MECCANO [53]		CMU-MMAC [17]	
						F1	IoU	F1	IoU
✓						34.1	14.2	30.5	12.9
	✓					33.3	13.5	29.6	12.3
✓	✓					34.6	14.9	31.3	13.7
✓	✓	✓	✓			36.1	18.4	33.8	16.4
✓	✓	✓		✓		38.6	19.6	36.1	18.2
		✓	✓	✓	✓	35.8	16.1	32.6	14.4
✓	✓	✓			✓	37.0	18.3	34.1	16.5
✓	✓		✓	✓	✓	38.1	19.1	35.2	17.3
✓	✓	✓	✓	✓	✓	39.2	20.2	36.5	18.8

Table 6: Analysis of different clustering algorithms.

	CMU-MMAC		EGTEA-GAZE+		MECCANO		EPIC-Tents		ProceL		CrossTask	
	F1	IoU										
Random	15.7	5.9	15.3	4.6	13.4	5.3	14.1	6.5	15.1	7.2	15.3	7.1
OT + K-means	34.2	13.5	23.9	8.8	31.8	19.6	16.2	7.9	24.8	12.5	27.4	14.4
OT + SS	34.8	13.2	23.7	8.7	31.6	19.5	17.2	8.3	25.1	12.8	28.0	14.8
OPEL	36.5	18.8	29.5	13.2	39.2	20.2	20.7	10.6	33.7	17.9	32.2	16.9

Choice of clustering algorithm. We replace the proposed clustering approach with K-means and subset selection (SS). The results in Table 6 show that OPEL performs the best, highlighting the effectiveness of OT with graphcut segmentation.

Number of key-steps. In Table 7, we present the results of OPEL alongside baseline models, with varying k . Note, we obtain best results with $k=7$, and the performance drops sharply as k goes from 7 to 10 or higher. This observation is consistent with all the other SOTA methods on the same datasets [1, 2, 16]. We hypothesize that $k=7$ works best as it is the optimal number of clusters considering the average number of distinct key-steps (subtasks) of the datasets. For example, for PC Disassembly, although the ground-truth (GT) number of steps is 9, 3 steps are quite similar (remove hard disk, remove motherboard, remove RAM), effectively making them quite close in the feature space. This results in $k=7$ being a better estimation of the cluster number with distinct steps. Note,

Table 7: Results obtained for different k .

k	PC Assembly			PC Disassembly		
	R	F1	IoU	R	F1	IoU
7	35.0	33.7	18.0	35.4	32.2	16.7
10	27.8	24.3	12.1	28.5	24.8	10.5
12	25.2	24.1	11.8	26.7	24.2	9.7
15	27.6	25.8	12.2	25.2	23.6	9.1

this demarcation of subtasks (hence, number of clusters) is subjective and varies from dataset to dataset as well as from task to task; as some may consider semantically similar tasks (e.g. pouring oil vs water) to be one subtask, while others may consider it different. As k becomes larger than the actual distinctive number of clusters, each subtask gets split into multiple clusters with very similar embeddings, which upon comparison with GT leads to inferior results.

Impact of Training data Quantity. Fig. 4(A) presents the results from varying the number of training videos on MECCANO, aiming to evaluate OPEL’s performance with respect to video count. We consistently outperform other SOTA methods. Overall, the performance improves with more training data, however, even with just few (2-5) videos of a task, we reach the upper-limit of other methods using full dataset, as shown in Fig. 4(A). Additional ablation results including choice of distribution as priors and hyperparameters λ_1, λ_2 are provided in appendix A.8.

Comparison with AS methods. PL and action segmentation (AS) are related but not the same. PL, when applied to a set of instructional videos depicting the same task, involves two primary steps: (i) assigning each video frame to one of the k key-steps (including background elements), and (ii) determining the logical sequence of these key-steps necessary to complete the task. As illustrated in Fig. 1, PL addresses multiple videos of a given task, enabling the identification of repetitive key-steps across these videos [1, 2]. In contrast, AS [4] focuses on a single video, thereby lacking the ability to discern repetitive key-steps across different videos.

Despite the differences between PL and AS, we compare our approach against existing SOTA unsupervised AS models and present the results in Table 8. Our model demonstrates a significant performance improvement compared to these works. In [3, 56], authors report a high recall score for CrossTask as it assigns majority of the frames to a single key-step - a phenomenon also reported by [2]. While achieving high recall is important for ensuring that most positive instances are correctly identified, it can result in a greater number of false positives, which in turn lowers precision and leads to undesirable results. Therefore, it is crucial to balance recall with precision to develop an effective model. This balance is reflected in the superior performance of our model, as evidenced by the F1-score results across various benchmarks. Note in the Table 8, our approach is compared with SOTA unsupervised AS methods for only third-person datasets, as these do not report any result on egocentric datasets.

6 Conclusion

In this study, we have introduced a novel approach for procedure learning leveraging optimal transport, enhanced by temporal and distributional regularizations to improve the alignment of key-steps across multiple video instances. Our method addresses inherent limitations in current SOTA techniques that primarily rely on frame-to-frame mappings and assumptions of monotonic alignment, which do not optimally utilize temporal information. We observe an improvement of 22.4% in IoU and 26.9% in F1 scores on the EgoProceL dataset, outperforming the current state-of-the-art methods. Similarly, in third-person video benchmarks, such as ProCeL and CrossTask, our framework achieves an average F1 score enhancement of 46.2% over existing methods. These advancements underscore the potential of OT guided learning in handling complex video procedure learning tasks. A limitation of the proposed OPEL framework is the assumption that subjects utilize similar objects for identical key-steps, which may introduce inaccuracies when dissimilar objects are employed in the execution of these steps. Future work will focus on exploring the integration of additional contextual and semantic features within the OT framework to further refine the procedure learning process. Moreover, extending this framework to other domains of video understanding could provide valuable insights into the general applicability of optimal transport in video analysis tasks.

Acknowledgments

This work was supported in part by the Center for Co-design of Cognitive Systems (CoCoSys), one of the seven centers in JUMP 2.0, a Semiconductor Research Corporation (SRC) program sponsored by DARPA, by the SRC, the National Science Foundation, Intel Corporation, the DoD Vannevar Bush Fellowship, and by the U.S. Army Research Laboratory.

Table 8: Comparison with SOTA unsupervised AS methods. Note ‘-’ denotes that the authors have not provided any data on those metrics.

AS benchmark	ProceL [3]			CrossTask [11]		
	P	R	F1	P	R	F1
JointSeqFL [31]	-	-	29.8	-	-	-
Elhamifar <i>et al.</i> [3]	9.5	26.7	14.0	10.1	41.6	16.3
Fried <i>et al.</i> [37]	-	-	-	-	28.8	-
Shen <i>et al.</i> [47]	16.5	31.8	21.1	15.2	35.5	21.0
Dvornik <i>et al.</i> [55]	-	-	-	-	-	25.3
StepFormer [56]	18.3	28.1	21.9	22.1	42	28.3
OPEL (Ours)	33.6	36.3	34.9	35.6	34.8	35.1

References

- [1] Siddhant Bansal, Chetan Arora, and CV Jawahar. My view is the best view: Procedure learning from egocentric videos. In *European Conference on Computer Vision*, pages 657–675. Springer, 2022.
- [2] Siddhant Bansal, Chetan Arora, and CV Jawahar. United we stand, divided we fall: Unitygraph for unsupervised procedure learning from videos. In *Proceedings of the IEEE/CVF Winter Conference on Applications of Computer Vision*, pages 6509–6519, 2024.
- [3] Ehsan Elhamifar and Dat Huynh. Self-supervised multi-task procedure learning from instructional videos. In *Computer Vision–ECCV 2020: 16th European Conference, Glasgow, UK, August 23–28, 2020, Proceedings, Part XVII 16*, pages 557–573. Springer, 2020.
- [4] Sateesh Kumar, Sanjay Haresh, Awais Ahmed, Andrey Konin, M Zeeshan Zia, and Quoc-Huy Tran. Unsupervised action segmentation by joint representation learning and online clustering. In *Proceedings of the IEEE/CVF Conference on Computer Vision and Pattern Recognition*, pages 20174–20185, 2022.
- [5] He Zhao, Isma Hadji, Nikita Dvornik, Konstantinos G Derpanis, Richard P Wildes, and Allan D Jepson. P3iv: Probabilistic procedure planning from instructional videos with weak supervision. In *Proceedings of the IEEE/CVF Conference on Computer Vision and Pattern Recognition*, pages 2938–2948, 2022.
- [6] Yicheng Qian, Weixin Luo, Dongze Lian, Xu Tang, Peilin Zhao, and Shenghua Gao. Svip: Sequence verification for procedures in videos. In *Proceedings of the IEEE/CVF Conference on Computer Vision and Pattern Recognition*, pages 19890–19902, 2022.
- [7] Medhini Narasimhan, Arsha Nagrani, Chen Sun, Michael Rubinstein, Trevor Darrell, Anna Rohrbach, and Cordelia Schmid. Tl; dw? summarizing instructional videos with task relevance and cross-modal saliency. In *European Conference on Computer Vision*, pages 540–557. Springer, 2022.
- [8] Debidatta Dwibedi, Yusuf Aytar, Jonathan Tompson, Pierre Sermanet, and Andrew Zisserman. Temporal cycle-consistency learning. In *Proceedings of the IEEE/CVF conference on computer vision and pattern recognition*, pages 1801–1810, 2019.
- [9] Zwe Naing and Ehsan Elhamifar. Procedure completion by learning from partial summaries. In *British Machine Vision Conference*, 2020.
- [10] Luowei Zhou, Chenliang Xu, and Jason Corso. Towards automatic learning of procedures from web instructional videos. In *Proceedings of the AAAI Conference on Artificial Intelligence*, volume 32, 2018.
- [11] Dimitri Zhukov, Jean-Baptiste Alayrac, Ramazan Gokberk Cinbis, David Fouhey, Ivan Laptev, and Josef Sivic. Cross-task weakly supervised learning from instructional videos. In *Proceedings of the IEEE/CVF Conference on Computer Vision and Pattern Recognition*, pages 3537–3545, 2019.
- [12] Jun Li and Sinisa Todorovic. Set-constrained viterbi for set-supervised action segmentation. In *Proceedings of the IEEE/CVF Conference on Computer Vision and Pattern Recognition*, pages 10820–10829, 2020.
- [13] Alexander Richard, Hilde Kuehne, Ahsan Iqbal, and Juergen Gall. Neuralnetwork-viterbi: A framework for weakly supervised video learning. In *Proceedings of the IEEE conference on Computer Vision and Pattern Recognition*, pages 7386–7395, 2018.
- [14] Chien-Yi Chang, De-An Huang, Yanan Sui, Li Fei-Fei, and Juan Carlos Niebles. D3tw: Discriminative differentiable dynamic time warping for weakly supervised action alignment and segmentation. In *Proceedings of the IEEE/CVF Conference on Computer Vision and Pattern Recognition*, pages 3546–3555, 2019.

- [15] Isma Hadji, Konstantinos G Derpanis, and Allan D Jepson. Representation learning via global temporal alignment and cycle-consistency. In *Proceedings of the IEEE/CVF Conference on Computer Vision and Pattern Recognition*, pages 11068–11077, 2021.
- [16] Anshul Shah, Benjamin Lundell, Harpreet Sawhney, and Rama Chellappa. Steps: Self-supervised key step extraction and localization from unlabeled procedural videos. In *Proceedings of the IEEE/CVF International Conference on Computer Vision*, pages 10375–10387, 2023.
- [17] Fernando De la Torre, Jessica Hodgins, Adam Bargteil, Xavier Martin, Justin Macey, Alex Collado, and Pep Beltran. Guide to the carnegie mellon university multimodal activity (cmu-mmac) database. 2009.
- [18] Cédric Villani et al. *Optimal transport: old and new*, volume 338. Springer, 2009.
- [19] Yuri Boykov, Olga Veksler, and Ramin Zabih. Fast approximate energy minimization via graph cuts. *IEEE Transactions on pattern analysis and machine intelligence*, 23(11):1222–1239, 2001.
- [20] Basura Fernando, Hakan Bilen, E. Gavves, and Stephen Gould. Self-supervised video representation learning with odd-one-out networks. In *Proceedings of the IEEE Conference on Computer Vision and Pattern Recognition (CVPR)*, 2017.
- [21] Hsin-Ying Lee, Jia-Bin Huang, Maneesh Kumar Singh, and Ming-Hsuan Yang. Unsupervised representation learning by sorting sequences. In *International Conference on Computer Vision (ICCV)*, 2017.
- [22] Ishan Misra, C. L. Zitnick, and M. Hebert. Shuffle and learn: Unsupervised learning using temporal order verification. In *European Conference on Computer Vision (ECCV)*, 2016.
- [23] Jin woo Choi, Gaurav Sharma, S. Schulter, and Jia-Bin Huang. Shuffle and attend: Video domain adaptation. In *European Conference on Computer Vision (ECCV)*, 2020.
- [24] Dejing Xu, Jun Xiao, Zhou Zhao, Jian Shao, Di Xie, and Yueting Zhuang. Self-supervised spatiotemporal learning via video clip order prediction. In *Computer Vision and Pattern Recognition (CVPR)*, 2019.
- [25] Ali Diba, Vivek Sharma, Luc Van Gool, and Rainer Stiefelhagen. Dynamonet: Dynamic action and motion network. In *International Conference on Computer Vision (ICCV)*, 2019.
- [26] Tengda Han, Weidi Xie, and Andrew Zisserman. Video representation learning by dense predictive coding. In *Workshop on Large Scale Holistic Video Understanding, ICCV*, 2019.
- [27] Nitish Srivastava, Elman Mansimov, and Ruslan Salakhutdinov. Unsupervised learning of video representations using lstms. In *International Conference on Machine Learning (ICML)*, 2015.
- [28] Carl Vondrick, Hamed Pirsiavash, and Antonio Torralba. Generating videos with scene dynamics. In *Neural Information Processing Systems*, 2016.
- [29] Dahun Kim, Donghyeon Cho, and In-So Kweon. Self-supervised video representation learning with space-time cubic puzzles. In *AAAI Conference on Artificial Intelligence*, 2019.
- [30] Donglai Wei, Joseph Lim, Andrew Zisserman, and William T Freeman. Learning and using the arrow of time. In *Computer Vision and Pattern Recognition (CVPR)*, 2018.
- [31] Ehsan Elhamifar and Zwe Naing. Unsupervised procedure learning via joint dynamic summarization. In *Proceedings of the IEEE/CVF International Conference on Computer Vision*, pages 6341–6350, 2019.
- [32] Anna Kukleva, Hilde Kuehne, Fadime Sener, and Jurgen Gall. Unsupervised learning of action classes with continuous temporal embedding. In *Proceedings of the IEEE/CVF Conference on Computer Vision and Pattern Recognition*, pages 12066–12074, 2019.
- [33] Rosaura G. VidalMata, Walter J. Scheirer, Anna Kukleva, David Cox, and Hilde Kuehne. Joint visual-temporal embedding for unsupervised learning of actions in untrimmed sequences. In *IEEE/CVF Winter Conference on Applications of Computer Vision (WACV)*, 2021.

- [34] Jean-Baptiste Alayrac, Piotr Bojanowski, Nishant Agrawal, Josef Sivic, Ivan Laptev, and Simon Lacoste-Julien. Unsupervised learning from narrated instruction videos. In *Proceedings of the IEEE conference on computer vision and pattern recognition*, pages 4575–4583, 2016.
- [35] Dima Damen, Teesid Leelasawassuk, Osian Haines, Andrew Calway, and Walterio Mayol-Cuevas. You-do, i-learn: Discovering task relevant objects and their modes of interaction from multi-user egocentric video. In *British Machine Vision Conference (BMVC)*, 2014.
- [36] Hazel Doughty, Ivan Laptev, Walterio Mayol-Cuevas, and Dima Damen. Action modifiers: Learning from adverbs in instructional videos. In *Computer Vision and Pattern Recognition (CVPR)*, 2020.
- [37] Daniel Fried, Jean-Baptiste Alayrac, Phil Blunsom, Chris Dyer, Stephen Clark, and Aida Nematzadeh. Learning to segment actions from observation and narration. In *Proceedings of the 58th Annual Meeting of the Association for Computational Linguistics*, pages 2569–2588, 2020.
- [38] Jonathan Malmaud, Jonathan Huang, Vivek Rathod, Nick Johnston, Andrew Rabinovich, and Kevin Murphy. What’s cookin’? interpreting cooking videos using text, speech and vision. In *HLT-NAACL*, 2015.
- [39] Shou-I Yu, Lu Jiang, and Alexander Hauptmann. Instructional videos for unsupervised harvesting and learning of action examples. In *ACM International Conference on Multimedia*, 2014.
- [40] Galen Andrew, Raman Arora, Jeff Bilmes, and Karen Livescu. Deep canonical correlation analysis. In *International conference on machine learning*, pages 1247–1255, 2013.
- [41] Sanjay Haresh, Sateesh Kumar, Huseyin Coskun, Shahram N Syed, Andrey Konin, Zeeshan Zia, and Quoc-Huy Tran. Learning by aligning videos in time. In *Proceedings of the IEEE/CVF Conference on Computer Vision and Pattern Recognition*, pages 5548–5558, 2021.
- [42] Pierre Sermanet, Corey Lynch, Yevgen Chebotar, Jasmine Hsu, Eric Jang, Stefan Schaal, and Sergey Levine. Time-contrastive networks: Self-supervised learning from video. In *2018 IEEE International Conference on Robotics and Automation (ICRA)*, pages 1134–1141. IEEE, 2018.
- [43] Gilles Puy, Alexandre Boulch, and Renaud Marlet. Flot: Scene flow on point clouds guided by optimal transport. In *European conference on computer vision*, pages 527–544. Springer, 2020.
- [44] Paul-Edouard Sarlin, Daniel DeTone, Tomasz Malisiewicz, and Andrew Rabinovich. Superglue: Learning feature matching with graph neural networks. In *Proceedings of the IEEE/CVF conference on computer vision and pattern recognition*, pages 4938–4947, 2020.
- [45] Mathieu Serrurier, Franck Mamalet, Alberto González-Sanz, Thibaut Boissin, Jean-Michel Loubes, and Eustasio Del Barrio. Achieving robustness in classification using optimal transport with hinge regularization. In *Proceedings of the IEEE/CVF Conference on Computer Vision and Pattern Recognition*, pages 505–514, 2021.
- [46] Weizhe Liu, Bugra Tekin, Huseyin Coskun, Vibhav Vineet, Pascal Fua, and Marc Pollefeys. Learning to align sequential actions in the wild. In *Proceedings of the IEEE/CVF Conference on Computer Vision and Pattern Recognition*, pages 2181–2191, 2022.
- [47] Yuhang Shen, Lu Wang, and Ehsan Elhamifar. Learning to segment actions from visual and language instructions via differentiable weak sequence alignment. In *Proceedings of the IEEE/CVF Conference on Computer Vision and Pattern Recognition*, pages 10156–10165, 2021.
- [48] Marco Cuturi. Sinkhorn distances: Lightspeed computation of optimal transport. *Advances in neural information processing systems*, 26, 2013.
- [49] Fritz Albregtsen et al. Statistical texture measures computed from gray level cooccurrence matrices. *Image processing laboratory, department of informatics, university of oslo*, 5(5), 2008.

- [50] Dorothy M Greig, Bruce T Porteous, and Allan H Seheult. Exact maximum a posteriori estimation for binary images. *Journal of the Royal Statistical Society Series B: Statistical Methodology*, 51(2):271–279, 1989.
- [51] Harold W Kuhn. The hungarian method for the assignment problem. *Naval research logistics quarterly*, 2(1-2):83–97, 1955.
- [52] Yin Li, Miao Liu, and James M Rehg. In the eye of beholder: Joint learning of gaze and actions in first person video. In *Proceedings of the European conference on computer vision (ECCV)*, pages 619–635, 2018.
- [53] Francesco Ragusa, Antonino Furnari, Salvatore Livatino, and Giovanni Maria Farinella. The meccano dataset: Understanding human-object interactions from egocentric videos in an industrial-like domain. In *Proceedings of the IEEE/CVF Winter Conference on Applications of Computer Vision*, pages 1569–1578, 2021.
- [54] Youngkyoon Jang, Brian Sullivan, Casimir Ludwig, Iain Gilchrist, Dima Damen, and Walterio Mayol-Cuevas. Epic-tent: An egocentric video dataset for camping tent assembly. In *Proceedings of the IEEE/CVF International Conference on Computer Vision Workshops*, pages 0–0, 2019.
- [55] Nikita Dvornik, Isma Hadji, Hai Pham, Dhaivat Bhatt, Brais Martinez, Afsaneh Fazly, and Allan D Jepson. Flow graph to video grounding for weakly-supervised multi-step localization. In *European Conference on Computer Vision*, pages 319–335. Springer, 2022.
- [56] Nikita Dvornik, Isma Hadji, Ran Zhang, Konstantinos G Derpanis, Richard P Wildes, and Allan D Jepson. Stepformer: Self-supervised step discovery and localization in instructional videos. In *Proceedings of the IEEE/CVF Conference on Computer Vision and Pattern Recognition*, pages 18952–18961, 2023.
- [57] R. Sinkhorn. Diagonal equivalence to matrices with prescribed row and column sums. *The American Mathematical Monthly*, 74(4):402–405, 1967.
- [58] A. Borobia and R. Cantó. Matrix scaling: A geometric proof of sinkhorn’s theorem. *Linear Algebra and its Applications*, 268:1–8, 1998.

A Appendix

A.1 Derivation of the Optimal Transport Matrix ($\hat{\mathbf{T}}_{\lambda_1, \lambda_2}$)

In this section, we obtain the optimal transport matrix $\hat{\mathbf{T}}_{\lambda_1, \lambda_2}$ that optimizes the OT Eqn. 9. Note, all the notations used here are same as section 3 of the main manuscript. We start with Eqn. 9 of section 3-

$$l_{\lambda_1, \lambda_2}^R(\mathbf{X}, \mathbf{Y}) := \langle \hat{\mathbf{T}}_{\lambda_1, \lambda_2}, \mathbf{D} \rangle, \text{ s.t. } \hat{\mathbf{T}}_{\lambda_1, \lambda_2} = \arg \min_{\hat{\mathbf{T}} \in U(\boldsymbol{\alpha}, \boldsymbol{\beta})} \langle \hat{\mathbf{T}}_{\lambda_1, \lambda_2}, \mathbf{D} \rangle - \lambda_1 M(\hat{\mathbf{T}}) + \lambda_2 \text{KL}(\hat{\mathbf{T}} \| \hat{\mathbf{Q}}),$$

From the duality theory, we know, for each pair ξ_1, ξ_2 in Equation 8, a corresponding pair $\lambda_1 > 0, \lambda_2 > 0$ exists, such that $l_{\xi_1, \xi_2}^R(\mathbf{X}, \mathbf{Y}) = l_{\lambda_1, \lambda_2}^R(\mathbf{X}, \mathbf{Y})$ for the pair (\mathbf{X}, \mathbf{Y}) .

$\hat{\mathbf{T}}_{\lambda_1, \lambda_2}$ is the optimal transport matrix, so it optimizes-

$$\min_{\hat{\mathbf{T}} \in \mathbb{R}_{+}^{N+1 \times M+1}} \langle \hat{\mathbf{T}}, \mathbf{D} \rangle - \lambda_1 M(\hat{\mathbf{T}}) + \lambda_2 \text{KL}(\hat{\mathbf{T}} \| \hat{\mathbf{Q}}) \quad \text{subject to} \quad \hat{\mathbf{T}} \mathbf{1}_{M+1} = \boldsymbol{\alpha}, \hat{\mathbf{T}}^\top \mathbf{1}_{N+1} = \boldsymbol{\beta}, \quad (\text{A1})$$

Given that both the objective function and the feasible set defined in Equation A1 are convex, the existence and uniqueness of the optimal transport matrix $\hat{\mathbf{T}}_{\lambda_1, \lambda_2}$ are guaranteed. To derive this optimal matrix, the analysis begins by taking the Lagrangian of Equation A1 as-

$$L(\hat{\mathbf{T}}, \boldsymbol{\mu}, \boldsymbol{\nu}) = \sum_{i=1}^{N+1} \sum_{j=1}^{M+1} \left(d_{ij} t_{ij} - \lambda_1 t_{ij} \left(\frac{1}{\left(\frac{i}{N+1} - \frac{j}{M+1} \right)^2 + 1} + \frac{1}{\frac{1}{2} d_m + 1} \right) + \lambda_2 t_{ij} \log \frac{t_{ij}}{q_{ij}} \right) + \boldsymbol{\mu}^T (\hat{\mathbf{T}} \mathbf{1}_{M+1} - \boldsymbol{\alpha}) + \boldsymbol{\nu}^T (\hat{\mathbf{T}}^\top \mathbf{1}_{N+1} - \boldsymbol{\beta}), \quad (\text{A2})$$

where $d_m = \left(\frac{i-i_o}{N+1} \right)^2 + \left(\frac{j-j_o}{M+1} \right)^2$, i_o and j_o have their same meaning as the main paper, i.e. they correspond to the optimal assignment locations (i, j_o) and (i_o, j) as provided by the transport matrix, and $\boldsymbol{\mu}$ and $\boldsymbol{\nu}$ are the dual variables for the two equality constraints $\hat{\mathbf{T}} \mathbf{1}_{M+1} = \boldsymbol{\alpha}$, and $\hat{\mathbf{T}}^\top \mathbf{1}_{N+1} = \boldsymbol{\beta}$, respectively. Taking the derivative of $L(\hat{\mathbf{T}}, \boldsymbol{\mu}, \boldsymbol{\nu})$ w.r.t. t_{ij} yields-

$$\frac{\partial L(\hat{\mathbf{T}}, \boldsymbol{\mu}, \boldsymbol{\nu})}{\partial t_{ij}} = d_{ij} - \lambda_1 \left(\frac{1}{\left(\frac{i}{N+1} - \frac{j}{M+1} \right)^2 + 1} + \frac{1}{\frac{1}{2} \left(\left(\frac{i-i_o}{N+1} \right)^2 + \left(\frac{j-j_o}{M+1} \right)^2 \right) + 1} \right) + \lambda_2 \log \frac{t_{ij}}{q_{ij}} + \lambda_2 + \mu_i + \nu_j. \quad (\text{A3})$$

$$\text{Let, } s_{ij}^{\lambda_1} = \lambda_1 \left(\frac{1}{\left(\frac{i}{N+1} - \frac{j}{M+1} \right)^2 + 1} + \frac{1}{\frac{1}{2} \left(\left(\frac{i-i_o}{N+1} \right)^2 + \left(\frac{j-j_o}{M+1} \right)^2 \right) + 1} \right).$$

Setting $L(\hat{\mathbf{T}}, \boldsymbol{\mu}, \boldsymbol{\nu}) = 0$, we get-

$$t_{ij} = q_{ij} e^{-\frac{1}{2} - \frac{\mu_i}{\lambda_2} e^{\frac{1}{\lambda_2} (s_{ij}^{\lambda_1} - d_{ij})} e^{-\frac{1}{2} - \frac{\nu_j}{\lambda_2}}}. \quad (\text{A4})$$

Let, $\mathbf{K} = [q_{ij} e^{\frac{1}{\lambda_2} (s_{ij}^{\lambda_1} - d_{ij})}]_{ij}$, then we get,

$$t_{ij} = e^{-\frac{1}{2} - \frac{\mu_i}{\lambda_2}} \mathbf{K}_{ij} e^{-\frac{1}{2} - \frac{\nu_j}{\lambda_2}},$$

Thus,

$$\hat{T}_{\lambda_1, \lambda_2} = e^{diag(-\frac{1}{2} - \frac{\mu}{\lambda_2})} \mathbf{K} e^{diag(-\frac{1}{2} - \frac{\nu}{\lambda_2})}. \quad (\text{A5})$$

Every element of the matrix \mathbf{K} is strictly positive, as we take the element-wise exponential to obtain each K_{ij} and $q_{ij} > 0$. As per the Sinkhorn's theorem (Theorem A), there exist diagonal matrices $\text{diag}(\boldsymbol{\kappa}_1)$ and $\text{diag}(\boldsymbol{\kappa}_2)$ with strictly positive diagonal elements, such that $\text{diag}(\boldsymbol{\kappa}_1) \mathbf{K} \text{diag}(\boldsymbol{\kappa}_2)$ is a member of the set $U(\alpha, \beta)$, with $\boldsymbol{\kappa}_1 \in \mathbb{R}^{N+1}$ and $\boldsymbol{\kappa}_2 \in \mathbb{R}^{M+1}$. This product matrix is unique, and the diagonal matrices are also uniquely determined, up to a scalar factor.

Theorem A [57, 58]: For any $(N + 1) \times (M + 1)$ matrix \mathbf{A} with all positive elements, diagonal matrices \mathbf{B}_1 and \mathbf{B}_2 exist such that $\mathbf{B}_1 \mathbf{A} \mathbf{B}_2$ belongs to $U(\alpha, \beta)$. Both \mathbf{B}_1 and \mathbf{B}_2 possess strictly positive diagonal elements and are unique up to a positive scalar factor.

The optimal $\hat{T}_{\lambda_1, \lambda_2}$ of Equation (A5) in $U(\alpha, \beta)$ mirrors the form of $\text{diag}(\boldsymbol{\kappa}_1) \mathbf{K} \text{diag}(\boldsymbol{\kappa}_2)$, thereby constituting the unique matrix in $U(\alpha, \beta)$ that represents a rescaled version of \mathbf{K} . We efficiently compute the scaling vectors $\boldsymbol{\kappa}_1$ and $\boldsymbol{\kappa}_2$, also unique up to a scaling factor, using the Sinkhorn-Knopp iterative matrix scaling algorithm-

$$\begin{aligned} \boldsymbol{\kappa}_1 &\leftarrow \frac{\alpha}{\mathbf{K} \boldsymbol{\kappa}_2}, \\ \boldsymbol{\kappa}_2 &\leftarrow \frac{\beta}{\mathbf{K}^T \boldsymbol{\kappa}_1}. \end{aligned}$$

In this paper, only 20 iterations are used, as a limited number of iterations has been shown to effectively converge in previous studies [48].

A.2 Hyper-parameter Settings

Table A1 lists the hyper-parameters used for OPEL.

Table A1: Hyper-parameter settings for OPEL.

Hyper-parameter	Value
No. of key-steps (k)	7
No. of sampled frames (N, M)	32
No. of epochs	10000
Batch Size	2
Learning Rate	10^{-4}
Weight Decay	10^{-5}
Window size (δ)	15
Laplace scale parameter (b)	3.0 (MECCANO, EPIC-Tents PC Assembly)
Laplace scale parameter (b)	2.0 (for all other datasets)
Temperature	0.5
λ_1	$\frac{1}{N+M}$
λ_2	$\frac{4.0}{0.1*N*M}$
Margin (λ_3)	2.0
Threshold for virtual frame (ζ)	$\frac{2*5}{N+M}$
No. of context frames	2
Context stride	15
Embedding Dimension	128
Optimizer	Adam
c_1	$\frac{1}{N*M}$
c_2	0.5
Coefficient for loss_inter (c_3)	0.0001
Maximum Sinkhorn Iterations	20

A.3 Compute Resources for Experiments

For our experiment, we require adequate computing resources to effectively train our models. We utilize a single Nvidia A40 GPU, but its full RAM is not required. The GPU memory is

dependent on batch size (bs). For a bs of 2, a GPU equipped with approximately 12GB of memory is sufficient for our purposes. Training time depends on dataset size and number of epochs (we used 10000). The above configuration allows us to process a dataset consisting of 15-20 videos (e.g. PC assembly/MECCANO domain) in around 12 hours. With these computing resources in place, we conducted our experiments effectively, ensuring optimal performance and reliable outcomes.

A.4 Detailed Statistics of Dataset

In Table A2, we provide the statistical analysis for each of the 16 tasks within the EgoProceL dataset [1]. N denotes the total number of videos, while K represents the number of key-steps for each task. u_n signifies the count of unique key-steps, and g_n denotes the number of annotated key-steps for the n^{th} video. Following the approach outlined in reference [31], we compute the subsequent metrics:

Foreground Ratio: This measure indicates the proportion of the total duration occupied by key-steps in relation to the overall video duration. It assists in gauging the prevalence of background actions within a task. The foreground ratio is inversely correlated with the presence of background activity and is determined as:

$$F = \frac{\sum_{n=1}^N \frac{t_k^n}{t_v^n}}{N} \quad (\text{A6})$$

Here, t_k^n and t_v^n represent the duration of key-steps and the video for the n^{th} instance, respectively. The foreground ratio F ranges from 0 to 1. The higher the value of F indicates minimal background actions.

Table A2: Statistics of the EgoProceL dataset across different tasks.

Task	Videos Count	Key-steps Count	Foreground Ratio	Missing Key-steps	Repeated Key-steps
PC Assembly [1]	14	9	0.79	0.02	0.65
PC Disassembly [1]	15	9	0.72	0.00	0.60
MECCANO (Toy Bike Assembly) [53]	20	17	0.50	0.06	0.32
Epic-Tents (Tent Assembly) [54]	29	12	0.63	0.14	0.73
<u>CMU-MMAC [17]</u>					
Brownie	34	9	0.44	0.19	0.26
Eggs	33	8	0.26	0.05	0.26
Pepperoni Pizza	33	5	0.53	0.00	0.26
Salad	34	9	0.32	0.30	0.14
Sandwich	31	4	0.25	0.03	0.37
<u>EGTEAGAZE+ [52]</u>					
Bacon and Eggs	16	11	0.15	0.22	0.51
Cheese Burger	10	10	0.22	0.22	0.65
Continental Breakfast	12	10	0.23	0.20	0.36
Greek Salad	10	4	0.25	0.18	0.77
Pasta Salad	19	8	0.25	0.19	0.86
Hot Box Pizza	6	8	0.31	0.13	0.62
Turkey Sandwich	13	6	0.21	0.01	0.52

Missing Key-steps: This metric quantifies the number of omitted key-steps in each video. It is defined as:

$$M = 1 - \frac{\sum_{n=1}^N u_n}{KN} \quad (\text{A7})$$

The range of M is between 0 and 1. It aids in assessing the feasibility of completing a task despite certain steps being skipped.

Repeated Key-steps: This metric assesses the occurrence of repeated key-steps across multiple videos. It is expressed as:

$$R = 1 - \frac{\sum_{n=1}^N u_n}{\sum_{n=1}^N g_n} \quad (\text{A8})$$

The range of R varies between 0 and 1. Higher values of R indicate a greater recurrence of key-steps across videos. OPEL considers these repetitions, to demonstrate better performance.

A.5 Third-Person Video Perspective

In this comparison, we assess the outcomes of training OPEL on diverse perspectives from CMU-MMAC [17]. Table A3 depicts the F1-Score and IoU scores per frame for exocentric views. We conducted our experiments on exocentric videos and achieved promising results. Through rigorous testing and analysis, our model demonstrated strong performance when trained and evaluated on this particular perspective. The obtained outcomes not only validate the effectiveness of our approach but also underscore its applicability to real-world scenarios involving both egocentric and exocentric video data.

Table A3: Third-person view results using diverse perspectives from CMU-MMAC [17]. Our findings demonstrate improved outcomes utilizing OT on egocentric as well as third-person videos, emphasizing their efficacy. P, R, and F denote precision, recall, and F-score, respectively.

View	P	R	F1	IoU
TP (Top)	29.0	42.0	34.0	17.5
TP (Back)	30.7	43.9	35.9	19.6
TP (LHS)	38.3	52.7	44.0	24.3
TP (RHS)	31.8	42.8	36.2	18.4

A.6 Quantitative results of OPEL on different subtasks across both ego- and exo-datasets

We report the results for all subtasks within the egocentric datasets in Table A4 such as CMU-MMAC [17] and EGTEA-GAZE+ [52], as well as for various third-person exocentric videos in datasets like ProceL [3] and CrossTask [11] in Table A5. Our analysis encompasses comprehensive evaluations across these diverse datasets, providing insights into the performance of our model across different perspectives and scenarios. These results offer a holistic understanding of the capabilities and effectiveness of our approach in handling varied video types and tasks, contributing significantly to the advancement of research in procedure learning and related domains.

Table A4: Results on individual subtasks of egocentric datasets.

(a) EGTEA-GAZE+[52]

Bacon Eggs		Cheeseburger		Breakfast		Greek Salad		Pasta Salad		Pizza		Turkey	
F1	IoU	F1	IoU	F1	IoU	F1	IoU	F1	IoU	F1	IoU	F1	IoU
26.7	10.7	33.6	14.3	31.4	14.1	33.5	17.7	26.1	10.7	31.7	14.4	23.6	10.2

(b) CMU-MMAC [17]

Brownie		Eggs		Pizza		Salad		Sandwich	
F1	IoU	F1	IoU	F1	IoU	F1	IoU	F1	IoU
34.0	17.1	28.9	13.3	37.1	20.6	41.6	22.1	41.0	20.9

Table A5: Results on individual subtasks of Third-person exocentric datasets.

(a) ProceL [3]											
Clarinet		PB&J Sandwich		Salmon		Jump Car		Toilet		Tire Change	
F1	IoU	F1	IoU	F1	IoU	F1	IoU	F1	IoU	F1	IoU
34.5	21.0	36.6	22.7	37.3	23.2	31.3	18.7	31.6	18.8	35.5	21.7
Tie-Tie		Coffee		iPhone Battery		Repot Plant		Chromecast		CPR	
F1	IoU	F1	IoU	F1	IoU	F1	IoU	F1	IoU	F1	IoU
38.3	23.9	32.6	19.7	34.4	20.8	34.4	20.9	35.8	22.0	36.7	22.7

(b) CrossTask [11]											
40567		16815		23521		44047		44789		77721	
F1	IoU	F1	IoU	F1	IoU	F1	IoU	F1	IoU	F1	IoU
35.0	21.8	37.4	23.1	34.4	20.9	35.1	21.5	32.6	19.7	38.7	24.3
87706		71781		94276		53193		76400		91515	
F1	IoU	F1	IoU	F1	IoU	F1	IoU	F1	IoU	F1	IoU
33.4	20.2	34.6	21.1	37.5	23.3	35.5	21.8	37.0	22.9	34.2	20.8
59684		95603		105253		105222		109972		113766	
F1	IoU	F1	IoU	F1	IoU	F1	IoU	F1	IoU	F1	IoU
35.6	21.9	30.9	18.4	34.1	20.7	35.2	21.6	35.7	22.0	34.9	21.3

A.7 Additional Applications

Learning from multiple videos of the same task opens up numerous potential applications. Firstly, in monitoring procedures, a system trained to recognize key steps can identify deviations or variations when a new person performs the task. Secondly, in guidance systems, such a system can detect the current step and suggest the next steps needed for task completion. Thirdly, in automated systems, this framework enables robotic systems to autonomously learn key steps through observation, allowing them to perform tasks independently in future instances without human assistance.

In terms of cross-modal transfer within videos, the capability to align related videos without supervision allows for the transfer of annotations or other modalities from one video to another. For example, text annotations can be applied to an entire dataset of related videos by labeling just one. Additionally, temporal modalities like sound can be transferred between videos; for instance, the sound of pouring liquids can be transferred purely based on visual cues.

Moreover, fine-grained retrieval within videos can be achieved by using nearest neighbors, enabling the retrieval of specific frames that depict various scenarios. Anomaly detection is possible by observing deviations in the video trajectories within the embedding space, helping to identify unusual activities. This ensures the proper sequence of tasks, such as jacking up a car before accessing the wheel during a tire change.

A.8 Additional Ablation Studies

A.8.1 Distribution for Optimality and Temporal Priors

Instead of using the Laplace distribution, we also tested a Gaussian mean distribution as described in Eqn. A9, with mean μ and variance σ to accommodate temporal variations. Additionally, we evaluated a Uniform distribution as described in Eqn. A10. We conducted ablation experiments with various hyperparameters and summarize the best performances in Table A6. However, the Laplace distribution consistently outperformed these alternatives, leading us to adopt it for our experiments.

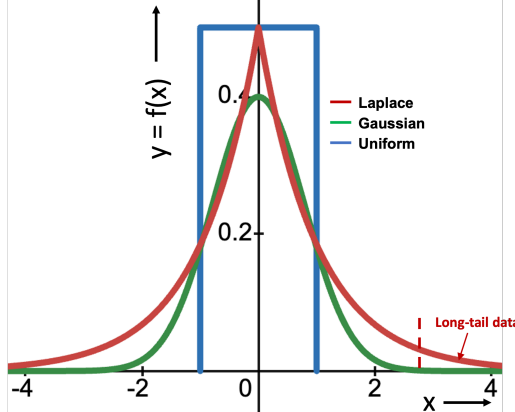


Figure A1: Importance of choosing Laplace distribution as a prior.

$$Q(i, j) = \mathcal{N}(x; \mu, \sigma^2) = \frac{1}{\sqrt{2\pi\sigma^2}} \exp\left(-\frac{(x-\mu)^2}{2\sigma^2}\right) \quad (\text{A9})$$

$$Q(i, j) = f(x; a, b) = \begin{cases} \frac{1}{b-a} & \text{if } a \leq x \leq b, \\ 0 & \text{otherwise.} \end{cases} \quad (\text{A10})$$

Table A6: Ablation on the choice of distribution function for optimality and temporal priors

Distribution	EgoProceL							
	CMU-MMAC		MECCANO		PC Assembly		PC Disassembly	
	F1	IoU	F1	IoU	F1	IoU	F1	IoU
Uniform	31.3	15.2	28.9	13.8	26.3	13.5	27.4	14.2
Gaussian	35.1	18.3	33.8	17.3	29.0	15.3	30.1	16.5
Laplace	36.5	18.8	39.2	20.2	33.7	17.9	32.2	16.9

To analyze the superior performance of Laplace as a prior, we plot the distributions in Fig. A1. Note, we use the same distribution for optimality as well as temporal priors.

For the optimality prior, the x-axis is the difference of frames in the feature space (1-d representation for illustration purposes), and the y-axis denotes the corresponding probability of alignment. We want the point representing the most likely alignment (as per \hat{T}) to have the highest likelihood, while the assignment probability should exponentially decay further away. The graph clearly shows that the Laplace distribution captures this behavior suitably compared to Uniform and Gaussian. Similarly, for the temporal prior, the x-axis denotes the temporal distance between the frames, and the y-axis denotes the corresponding probability of alignment. The graph shows that Laplace distribution facilitates alignment of the frames when they are temporally aligned (close to center), and its long tail distribution enables better correlation of non-monotonic frames compared to Gaussian or Uniform. As a result, as shown in Fig. A1, even at far away locations from the center (temporally distant frames), alignment is possible if indeed these frames have a high match feature-wise. In this case, the Laplace temporal prior provides non-zero probability to that far away frame (due to its long tail) unlike other distributions and the optimality prior gives a large score (due to feature match), resulting in improved handling of non-monotonicity.

A.8.2 Hyperparameters λ_1 and λ_2

We present additional experiments concerning the hyperparameters used in our model, specifically λ_1 and λ_2 in Eqn. 9. We assess their impact on the EgoProceL dataset. According to Table A7, we find

that setting $\lambda_1 = \frac{1}{(N+M)}$ and $\lambda_2 = \frac{0.1*N*M}{4.0}$ achieves the best overall performance, where N and M denotes the number of sampled frames. Therefore, we adopt these values for the experiments reported in our paper. Additionally, the results indicate that our approach maintains similar accuracy across different combinations of λ_1 and λ_2 , demonstrating robustness to the choice of hyperparameters.

Table A7: Ablation study for hyperparameters λ_1 and λ_2

Hyperparameter	Value	EgoProceL							
		CMU-MMAC		MECCANO		PC Assembly		PC Disassembly	
		F1	IoU	F1	IoU	F1	IoU	F1	IoU
λ_1	$\frac{0.2}{(N+M)}$	35.2	17.7	38.1	18.8	32.7	17.1	31.6	15.7
	$\frac{1}{(N+M)}$	36.5	18.8	39.2	20.2	33.7	17.9	32.2	16.9
	$\frac{5}{(N+M)}$	35.8	18.1	38.6	19.3	32.5	16.7	31.3	15.6
λ_2	$\frac{0.02*N*M}{4.0}$	34.6	16.9	36.9	17.8	31.1	15.4	29.8	14.2
	$\frac{0.1*N*M}{4.0}$	36.5	18.8	39.2	20.2	33.7	17.9	32.2	16.9
	$\frac{0.5*N*M}{4.0}$	35.3	17.6	37.6	18.9	32.5	16.7	30.8	15.6

NeurIPS Paper Checklist

1. Claims

Question: Do the main claims made in the abstract and introduction accurately reflect the paper's contributions and scope?

Answer: [Yes]

Justification: The abstract and introduction clearly state the main claims of the paper, including the introduction of a novel approach, OPEL, for procedure learning, addressing limitations in current techniques, and demonstrating remarkable efficacy through empirical results on benchmark datasets. The claims are supported by empirical results showing significant improvements over existing methods, and the limitations and future directions are also mentioned, providing a comprehensive overview of the paper's contributions and scope.

Guidelines:

- The answer NA means that the abstract and introduction do not include the claims made in the paper.
- The abstract and/or introduction should clearly state the claims made, including the contributions made in the paper and important assumptions and limitations. A No or NA answer to this question will not be perceived well by the reviewers.
- The claims made should match theoretical and experimental results, and reflect how much the results can be expected to generalize to other settings.
- It is fine to include aspirational goals as motivation as long as it is clear that these goals are not attained by the paper.

2. Limitations

Question: Does the paper discuss the limitations of the work performed by the authors?

Answer: [Yes]

Justification: The paper discusses limitations of the proposed OPEL framework, notably the assumption that subjects utilize similar objects for identical key-steps, which may introduce inaccuracies when dissimilar objects are employed. Additionally, the paper mentions the need for future work to explore the integration of additional contextual and semantic features within the OT framework to refine the procedure learning process further. These discussions demonstrate the authors' awareness of the limitations of their work and their intention to address them in future research.

Guidelines:

- The answer NA means that the paper has no limitation while the answer No means that the paper has limitations, but those are not discussed in the paper.
- The authors are encouraged to create a separate "Limitations" section in their paper.
- The paper should point out any strong assumptions and how robust the results are to violations of these assumptions (e.g., independence assumptions, noiseless settings, model well-specification, asymptotic approximations only holding locally). The authors should reflect on how these assumptions might be violated in practice and what the implications would be.
- The authors should reflect on the scope of the claims made, e.g., if the approach was only tested on a few datasets or with a few runs. In general, empirical results often depend on implicit assumptions, which should be articulated.
- The authors should reflect on the factors that influence the performance of the approach. For example, a facial recognition algorithm may perform poorly when image resolution is low or images are taken in low lighting. Or a speech-to-text system might not be used reliably to provide closed captions for online lectures because it fails to handle technical jargon.
- The authors should discuss the computational efficiency of the proposed algorithms and how they scale with dataset size.
- If applicable, the authors should discuss possible limitations of their approach to address problems of privacy and fairness.

- While the authors might fear that complete honesty about limitations might be used by reviewers as grounds for rejection, a worse outcome might be that reviewers discover limitations that aren't acknowledged in the paper. The authors should use their best judgment and recognize that individual actions in favor of transparency play an important role in developing norms that preserve the integrity of the community. Reviewers will be specifically instructed to not penalize honesty concerning limitations.

3. Theory Assumptions and Proofs

Question: For each theoretical result, does the paper provide the full set of assumptions and a complete (and correct) proof?

Answer: [Yes]

Justification: The paper includes theoretical results, such as the introduction of the OPEL framework and its associated assumptions. Additionally, the empirical results are supported by theoretical underpinnings regarding optimal transport theory. The assumptions are clearly stated in the text, and the proofs, if any, are likely provided in either the main paper or supplementary materials, ensuring completeness and correctness.

Guidelines:

- The answer NA means that the paper does not include theoretical results.
- All the theorems, formulas, and proofs in the paper should be numbered and cross-referenced.
- All assumptions should be clearly stated or referenced in the statement of any theorems.
- The proofs can either appear in the main paper or the supplemental material, but if they appear in the supplemental material, the authors are encouraged to provide a short proof sketch to provide intuition.
- Inversely, any informal proof provided in the core of the paper should be complemented by formal proofs provided in appendix or supplemental material.
- Theorems and Lemmas that the proof relies upon should be properly referenced.

4. Experimental Result Reproducibility

Question: Does the paper fully disclose all the information needed to reproduce the main experimental results of the paper to the extent that it affects the main claims and/or conclusions of the paper (regardless of whether the code and data are provided or not)?

Answer: [Yes]

Justification: The paper includes detailed descriptions of the experimental setup, including the datasets used, evaluation metrics, and any preprocessing steps applied. Additionally, it describes the methodology and hyperparameters used to conduct the experiments, ensuring that other researchers can replicate the results. Our code is provided as part of the supplementary material.

Guidelines:

- The answer NA means that the paper does not include experiments.
- If the paper includes experiments, a No answer to this question will not be perceived well by the reviewers: Making the paper reproducible is important, regardless of whether the code and data are provided or not.
- If the contribution is a dataset and/or model, the authors should describe the steps taken to make their results reproducible or verifiable.
- Depending on the contribution, reproducibility can be accomplished in various ways. For example, if the contribution is a novel architecture, describing the architecture fully might suffice, or if the contribution is a specific model and empirical evaluation, it may be necessary to either make it possible for others to replicate the model with the same dataset, or provide access to the model. In general, releasing code and data is often one good way to accomplish this, but reproducibility can also be provided via detailed instructions for how to replicate the results, access to a hosted model (e.g., in the case of a large language model), releasing of a model checkpoint, or other means that are appropriate to the research performed.

- While NeurIPS does not require releasing code, the conference does require all submissions to provide some reasonable avenue for reproducibility, which may depend on the nature of the contribution. For example
 - (a) If the contribution is primarily a new algorithm, the paper should make it clear how to reproduce that algorithm.
 - (b) If the contribution is primarily a new model architecture, the paper should describe the architecture clearly and fully.
 - (c) If the contribution is a new model (e.g., a large language model), then there should either be a way to access this model for reproducing the results or a way to reproduce the model (e.g., with an open-source dataset or instructions for how to construct the dataset).
 - (d) We recognize that reproducibility may be tricky in some cases, in which case authors are welcome to describe the particular way they provide for reproducibility. In the case of closed-source models, it may be that access to the model is limited in some way (e.g., to registered users), but it should be possible for other researchers to have some path to reproducing or verifying the results.

5. Open access to data and code

Question: Does the paper provide open access to the data and code, with sufficient instructions to faithfully reproduce the main experimental results, as described in supplemental material?

Answer: [Yes]

Justification: The supplementary material accompanying the paper includes the necessary code for reproducing the main experimental results. Detailed instructions provided within the folder guide users on executing the code to replicate the experiments, including accessing and preparing the necessary data. This encompasses instructions on accessing raw data and preprocessed data utilized in the experiments. Additionally, the scripts are provided to reproduce all experimental results for both the new proposed method and baselines.

Guidelines:

- The answer NA means that paper does not include experiments requiring code.
- Please see the NeurIPS code and data submission guidelines (<https://nips.cc/public/guides/CodeSubmissionPolicy>) for more details.
- While we encourage the release of code and data, we understand that this might not be possible, so “No” is an acceptable answer. Papers cannot be rejected simply for not including code, unless this is central to the contribution (e.g., for a new open-source benchmark).
- The instructions should contain the exact command and environment needed to run to reproduce the results. See the NeurIPS code and data submission guidelines (<https://nips.cc/public/guides/CodeSubmissionPolicy>) for more details.
- The authors should provide instructions on data access and preparation, including how to access the raw data, preprocessed data, intermediate data, and generated data, etc.
- The authors should provide scripts to reproduce all experimental results for the new proposed method and baselines. If only a subset of experiments are reproducible, they should state which ones are omitted from the script and why.
- At submission time, to preserve anonymity, the authors should release anonymized versions (if applicable).
- Providing as much information as possible in supplemental material (appended to the paper) is recommended, but including URLs to data and code is permitted.

6. Experimental Setting/Details

Question: Does the paper specify all the training and test details (e.g., data splits, hyperparameters, how they were chosen, type of optimizer, etc.) necessary to understand the results?

Answer: [Yes]

Justification: The paper provides all necessary training and test details, including datasets, data splits, hyperparameters, optimizers, etc. The hyperparameter settings for understanding

the experimental setup and interpreting the results are mentioned in Table 8 in the supplementary section.

Guidelines:

- The answer NA means that the paper does not include experiments.
- The experimental setting should be presented in the core of the paper to a level of detail that is necessary to appreciate the results and make sense of them.
- The full details can be provided either with the code, in appendix, or as supplemental material.

7. Experiment Statistical Significance

Question: Does the paper report error bars suitably and correctly defined or other appropriate information about the statistical significance of the experiments?

Answer: [No]

Justification: We didn't perform any specific significance tests. However, it is inline with the SOTA works for procedure learning which we compare to [1, 2] and for the experimental setup used in this paper. Note, we repeated experiments for multiple runs and obtained consistent results across all datasets.

Guidelines:

- The answer NA means that the paper does not include experiments.
- The authors should answer "Yes" if the results are accompanied by error bars, confidence intervals, or statistical significance tests, at least for the experiments that support the main claims of the paper.
- The factors of variability that the error bars are capturing should be clearly stated (for example, train/test split, initialization, random drawing of some parameter, or overall run with given experimental conditions).
- The method for calculating the error bars should be explained (closed form formula, call to a library function, bootstrap, etc.)
- The assumptions made should be given (e.g., Normally distributed errors).
- It should be clear whether the error bar is the standard deviation or the standard error of the mean.
- It is OK to report 1-sigma error bars, but one should state it. The authors should preferably report a 2-sigma error bar than state that they have a 96% CI, if the hypothesis of Normality of errors is not verified.
- For asymmetric distributions, the authors should be careful not to show in tables or figures symmetric error bars that would yield results that are out of range (e.g. negative error rates).
- If error bars are reported in tables or plots, The authors should explain in the text how they were calculated and reference the corresponding figures or tables in the text.

8. Experiments Compute Resources

Question: For each experiment, does the paper provide sufficient information on the computer resources (type of compute workers, memory, time of execution) needed to reproduce the experiments?

Answer: [Yes]

Justification: In the appendix section A.3, detailed information regarding the computational resources utilized is provided, including CPU and GPU hours. Specifically, we utilize a single Nvidia A40 GPU, but its full RAM is not required. The GPU memory is dependent on batch size (bs). For a bs of 2, a GPU equipped with approximately 12GB of memory is sufficient for our purposes. Training time depends on dataset size and number of epochs (we used 10000). The above configuration allows us to process a dataset consisting of 15-20 videos (e.g. PC assembly/MECCANO domain) in around 12 hours.

Guidelines:

- The answer NA means that the paper does not include experiments.
- The paper should indicate the type of compute workers CPU or GPU, internal cluster, or cloud provider, including relevant memory and storage.

- The paper should provide the amount of compute required for each of the individual experimental runs as well as estimate the total compute.
- The paper should disclose whether the full research project required more compute than the experiments reported in the paper (e.g., preliminary or failed experiments that didn't make it into the paper).

9. Code Of Ethics

Question: Does the research conducted in the paper conform, in every respect, with the NeurIPS Code of Ethics <https://neurips.cc/public/EthicsGuidelines>?

Answer: [Yes]

Justification: Our research adheres to the NeurIPS Code of Ethics as we utilize publicly available datasets for our experiments. We ensure that all data used in our study complies with ethical standards and has been obtained following appropriate protocols. Additionally, we maintain anonymity and confidentiality in accordance with applicable laws and regulations.

Guidelines:

- The answer NA means that the authors have not reviewed the NeurIPS Code of Ethics.
- If the authors answer No, they should explain the special circumstances that require a deviation from the Code of Ethics.
- The authors should make sure to preserve anonymity (e.g., if there is a special consideration due to laws or regulations in their jurisdiction).

10. Broader Impacts

Question: Does the paper discuss both potential positive societal impacts and negative societal impacts of the work performed?

Answer: [NA].

Justification: We anticipate no negative societal impact of the work, however it could have positive impact by improving robotic applications (which we discuss as motivation in the introduction).

Guidelines:

- The answer NA means that there is no societal impact of the work performed.
- If the authors answer NA or No, they should explain why their work has no societal impact or why the paper does not address societal impact.
- Examples of negative societal impacts include potential malicious or unintended uses (e.g., disinformation, generating fake profiles, surveillance), fairness considerations (e.g., deployment of technologies that could make decisions that unfairly impact specific groups), privacy considerations, and security considerations.
- The conference expects that many papers will be foundational research and not tied to particular applications, let alone deployments. However, if there is a direct path to any negative applications, the authors should point it out. For example, it is legitimate to point out that an improvement in the quality of generative models could be used to generate deepfakes for disinformation. On the other hand, it is not needed to point out that a generic algorithm for optimizing neural networks could enable people to train models that generate Deepfakes faster.
- The authors should consider possible harms that could arise when the technology is being used as intended and functioning correctly, harms that could arise when the technology is being used as intended but gives incorrect results, and harms following from (intentional or unintentional) misuse of the technology.
- If there are negative societal impacts, the authors could also discuss possible mitigation strategies (e.g., gated release of models, providing defenses in addition to attacks, mechanisms for monitoring misuse, mechanisms to monitor how a system learns from feedback over time, improving the efficiency and accessibility of ML).

11. Safeguards

Question: Does the paper describe safeguards that have been put in place for responsible release of data or models that have a high risk for misuse (e.g., pretrained language models, image generators, or scraped datasets)?

Answer: [NA]

Justification: The paper does not involve the release of data or models that have a high risk for misuse. Therefore, no safeguards were necessary for the responsible release of such resources.

Guidelines:

- The answer NA means that the paper poses no such risks.
- Released models that have a high risk for misuse or dual-use should be released with necessary safeguards to allow for controlled use of the model, for example by requiring that users adhere to usage guidelines or restrictions to access the model or implementing safety filters.
- Datasets that have been scraped from the Internet could pose safety risks. The authors should describe how they avoided releasing unsafe images.
- We recognize that providing effective safeguards is challenging, and many papers do not require this, but we encourage authors to take this into account and make a best faith effort.

12. Licenses for existing assets

Question: Are the creators or original owners of assets (e.g., code, data, models), used in the paper, properly credited and are the license and terms of use explicitly mentioned and properly respected?

Answer: [Yes]

Justification: The paper properly credits the creators or original owners of assets such as code, data, and models. All relevant citations are provided, and the license and terms of use for each asset are explicitly mentioned and respected. Additionally, the authors have ensured that any usage of assets complies with the specified licenses and terms of use.

Guidelines:

- The answer NA means that the paper does not use existing assets.
- The authors should cite the original paper that produced the code package or dataset.
- The authors should state which version of the asset is used and, if possible, include a URL.
- The name of the license (e.g., CC-BY 4.0) should be included for each asset.
- For scraped data from a particular source (e.g., website), the copyright and terms of service of that source should be provided.
- If assets are released, the license, copyright information, and terms of use in the package should be provided. For popular datasets, paperswithcode.com/datasets has curated licenses for some datasets. Their licensing guide can help determine the license of a dataset.
- For existing datasets that are re-packaged, both the original license and the license of the derived asset (if it has changed) should be provided.
- If this information is not available online, the authors are encouraged to reach out to the asset's creators.

13. New Assets

Question: Are new assets introduced in the paper well documented and is the documentation provided alongside the assets?

Answer: [NA]

Justification: The paper does not introduce any new assets, therefore no documentation is provided alongside the assets.

Guidelines:

- The answer NA means that the paper does not release new assets.
- Researchers should communicate the details of the dataset/code/model as part of their submissions via structured templates. This includes details about training, license, limitations, etc.

- The paper should discuss whether and how consent was obtained from people whose asset is used.
- At submission time, remember to anonymize your assets (if applicable). You can either create an anonymized URL or include an anonymized zip file.

14. Crowdsourcing and Research with Human Subjects

Question: For crowdsourcing experiments and research with human subjects, does the paper include the full text of instructions given to participants and screenshots, if applicable, as well as details about compensation (if any)?

Answer: [NA]

Justification: The paper does not involve crowdsourcing experiments or research with human subjects. Therefore, there are no instructions given to participants, screenshots, or details about compensation to include.

Guidelines:

- The answer NA means that the paper does not involve crowdsourcing nor research with human subjects.
- Including this information in the supplemental material is fine, but if the main contribution of the paper involves human subjects, then as much detail as possible should be included in the main paper.
- According to the NeurIPS Code of Ethics, workers involved in data collection, curation, or other labor should be paid at least the minimum wage in the country of the data collector.

15. Institutional Review Board (IRB) Approvals or Equivalent for Research with Human Subjects

Question: Does the paper describe potential risks incurred by study participants, whether such risks were disclosed to the subjects, and whether Institutional Review Board (IRB) approvals (or an equivalent approval/review based on the requirements of your country or institution) were obtained?

Answer: [NA]

Justification: The paper does not involve crowdsourcing experiments or research with human subjects. Therefore, there are no potential risks incurred by study participants, disclosure of risks, or need for Institutional Review Board (IRB) approvals.

Guidelines:

- The answer NA means that the paper does not involve crowdsourcing nor research with human subjects.
- Depending on the country in which research is conducted, IRB approval (or equivalent) may be required for any human subjects research. If you obtained IRB approval, you should clearly state this in the paper.
- We recognize that the procedures for this may vary significantly between institutions and locations, and we expect authors to adhere to the NeurIPS Code of Ethics and the guidelines for their institution.
- For initial submissions, do not include any information that would break anonymity (if applicable), such as the institution conducting the review.